

Modeling Powered Aerodynamics for the Orion Launch Abort Vehicle Aerodynamic Database (Invited)

David T. Chan* and Eric L. Walker†

NASA Langley Research Center, Hampton, VA, 23681

Philip E. Robinson‡ and Thomas M. Wilson§

NASA Johnson Space Center, Houston, TX, 77058

Modeling the aerodynamics of the Orion Launch Abort Vehicle (LAV) has presented many technical challenges to the developers of the Orion aerodynamic database. During a launch abort event, the aerodynamic environment around the LAV is very complex as multiple solid rocket plumes interact with each other and the vehicle. It is further complicated by vehicle separation events such as between the LAV and the launch vehicle stack or between the launch abort tower and the crew module. The aerodynamic database for the LAV was developed mainly from wind tunnel tests involving powered jet simulations of the rocket exhaust plumes, supported by computational fluid dynamic simulations. However, limitations in both methods have made it difficult to properly capture the aerodynamics of the LAV in experimental and numerical simulations. These limitations have also influenced decisions regarding the modeling and structure of the aerodynamic database for the LAV and led to compromises and creative solutions. Two database modeling approaches are presented in this paper (incremental aerodynamics and total aerodynamics), with examples showing strengths and weaknesses of each approach. In addition, the unique problems presented to the database developers by the large data space required for modeling a launch abort event illustrate the complexities of working with multi-dimensional data.

Nomenclature

Symbols			
		d	Distance between balance force gauges, inches
C_A	LAV axis axial force coefficient	F	Attitude control motor individual nozzle force, lbf
C_l	LAV axis rolling moment coefficient	F_{res}	Attitude control motor resultant force, lbf
C_m	LAV axis pitching moment coefficient	k	Data coverage factor
C_N	LAV axis normal force coefficient	M_{exit}	Jet exit Mach number
C_n	LAV axis yawing moment coefficient	MI	Margin Index
		N_1	Balance force gauge 1
C_T	Thrust coefficient	N_2	Balance force gauge 2
C_x	LAV axis generic force or moment coefficient ($C_A, C_N, C_m, C_Y, C_n,$ or C_l)	NF	Normal force, lbf
		PM	Pitching moment, in-lbf
		q_∞	Dynamic pressure, psf
C_Y	LAV axis side force coefficient		

*Research Aerospace Engineer. Configuration Aerodynamics Branch. NASA Langley Research Center. Member AIAA.

†Research Aerospace Engineer. Configuration Aerodynamics Branch. NASA Langley Research Center. Lifetime Senior Member AIAA.

‡Aerospace Engineer. EG311 Division. NASA Johnson Space Center.

§Aerospace Engineer. ERC Inc. NASA Johnson Space Center. Member AIAA.

S_{ref}	Vehicle reference area, ft ²	<i>boost</i>	Boost (AM+ACM) effect
SS	Sum of squares	<i>sep, separation</i>	Separation effect
T_{bal}	Thrust balance	<i>total</i>	Total effect
U	Total uncertainty	<i>unpowered</i>	Unpowered effect
u	Uncertainty component		
α	Angle of attack, deg	Units	
β	Angle of sideslip, deg	°, deg	degrees
Δ	denotes increment or difference	°F	degrees Fahrenheit
ΔX	Axial separation distance measured in CM heat shield diameters	atm	atmospheres
		ft ²	square feet
ΔY	Lateral separation distance measured in CM heat shield diameters	in-lbf	inch-pound force
		lbf	pounds force
ΔZ	Normal separation distance measured in CM heat shield diameters	psf	pounds per square foot
		psi	pounds per square inch
$\Delta\alpha$	Relative angle of attack difference between separating vehicles, deg	psia	pounds per square inch absolute
$\Delta\beta$	Relative angle of sideslip difference between separating vehicles, deg	sec	seconds
ϵ	Random number between -1 and 1 drawn from a uniform distribution	Acronyms	
γ_{jet}	Ratio of specific heats for a jet plume	ACM	Attitude Control Motor
ρ	Correlation parameter	AM	Abort Motor
σ	Standard deviation	API	Application Programming Interface
θ	Attitude control motor individual nozzle firing azimuth angle, deg	CAP	CEV Aerosciences Project
		CEV	Crew Exploration Vehicle
θ_{res}	Attitude control motor resultant firing azimuth angle, deg	CFD	Computational Fluid Dynamics
		CLV	Crew Launch Vehicle
θ_{thrust}	Attitude control motor resultant thrust azimuth angle, deg	CM	Crew Module
		DOF	Degrees of Freedom
Subscripts		GN&C	Guidance, Navigation, and Control
$()_{ACMsym}$	ACM Symmetry	ISS	International Space Station
$()_{Bal}$	Balance	ITAR	International Traffic in Arms Regulations
$()_{CFD}$	Computational Fluid Dynamics		
$()_{DBM}$	Database Model	JM	Jettison Motor
$()_{Interp}$	Interpolation	LAS	Launch Abort System
$()_{Rep}$	Repeatability	LAT	Launch Abort Tower
ACM, acm	ACM effect	LAV	Launch Abort Vehicle
AM	AM effect	LEO	Low-Earth Orbit
		MRC	Moment Reference Center
		NASA	National Aeronautics and Space Administration
		OML	Outer Mold Line
		SBU	Sensitive But Unclassified
		WT	Wind Tunnel

I. Introduction

THE Orion Crew Exploration Vehicle (CEV) was NASA's planned replacement for the Space Shuttle to carry future astronauts into orbit for missions to low-earth orbit (LEO) and the International Space Station (ISS) and for missions to the moon, to Mars, and beyond.¹ The CEV is similar in shape to the Apollo spacecraft, but significantly larger. The CEV was designed to launch atop the Ares I Crew Launch Vehicle (CLV), a two-stage booster employing both solid and liquid-fueled rocket motors. For crew safety, the CEV utilized a launch abort system (LAS) that is capable of pulling the Crew Module (CM) capsule away from the CLV in the event of an emergency on the launch pad or at any point along the ascent trajectory until nominal tower jettison. The combination of the LAS mated to the CM is referred to as the Launch

Abort Vehicle (LAV).

The LAV, shown in Fig. 1, consists of an ogive-conical fairing that surrounds the CM and connects to a cylindrical tower containing three solid rocket motors used during an abort. The abort motor (AM) is a high-thrust, high-impulse engine utilizing four exposed, reverse-flow nozzles to quickly pull the CM away from the CLV. The attitude control motor (ACM) is used to provide steering and control of the vehicle during an abort and consists of a single solid rocket motor connected to eight axisymmetric nozzles arranged circumferentially around the tower and perpendicular to the centerline axis of the vehicle. The jettison motor (JM) lies approximately in the middle of the tower and is used to pull the launch abort tower (LAT) away from the CM in the final stages of an abort before the CM begins its free-flight. The JM employs four nozzles that are scarfed flush with the surface of the tower.

A typical abort sequence is shown in Fig. 2. In the event of an emergency, the AM fires to pull the LAV away from the CLV while the ACM fires to provide steering and control. After the AM burns out, the vehicle continues to coast, with the ACM providing trim near zero angle of attack. The ACM then turns the LAV to a heat-shield-forward orientation, damping out pitch rates prior to tower jettison. Pyrotechnic bolts discharge to separate the LAT from the CM, while the JM fires nearly simultaneously to clear the LAT from the CM prior to parachute deployment. The entire abort sequence takes approximately 20-30 seconds to complete.

The Orion aerodynamic database has been developed by the CEV Aerosciences Project (CAP), and is regularly updated with improvements to the aerodynamic modeling of the various Orion vehicles (crew module, LAV, etc.) through the different flight phases. The database covers the aerodynamics of the CM for nominal on-orbit and atmospheric re-entry scenarios and covers the aerodynamics of the LAV, LAT, and CM for launch abort scenarios, beginning with separation from the launch vehicle to the point when the crew module lands safely.² It incorporates aerodynamic data primarily from wind tunnel (WT) testing and computational fluid dynamics (CFD) analyses. The primary function of the database is to provide aerodynamic data to the trajectory simulations that are used to develop the guidance, navigation, and control (GN&C) systems for the vehicles. The CAP team provides this data through an Application Programming Interface³ (API) that is integrated into the trajectory simulation tools. When invoked, the API computes and returns the aerodynamic forces and moments at the desired vehicle state.

The largest portion of the aerodynamic database is dedicated to the launch abort vehicle. Modeling the aerodynamics of the LAV as it travels through the abort trajectory is difficult because of the jet interaction effects between the multiple sets of solid rocket motor plumes and because of the two-body proximity effects during vehicle separation events. Furthermore, since the database covers all launch aborts from the pad to over Mach 7, it includes data over a large range of Mach numbers, vehicle attitudes and separation positions, and motor thrust levels. To simplify the problem, the database was developed with the philosophy that each major phase of the abort sequence was to be analyzed separately. Experimental and numerical simulations were conducted to model the aerodynamics of the LAV in each of the flight phases. However, due to the difficulties in simulating multiple jet plume and two-body proximity effects in both wind tunnel testing and CFD analyses and the need to obtain sufficient data to cover the large multi-dimensional data space under time and resource constraints, certain compromises were needed in the development and structure of the aerodynamic database. This paper will discuss the different approaches taken in modeling the aerodynamics of the LAV and the challenges in working within a large multi-dimensional data space.

The Orion LAV and its aerodynamics have been designated sensitive but unclassified (SBU) due to export control restrictions under the International Traffic in Arms Regulations (ITAR). Therefore, to comply with SBU rules, some details have been removed from plots and figures in this paper.

II. Powered Aerodynamics Modeling Approach

As the LAV travels through the different phases of the abort sequence (Fig. 2), at least one of the three sets of solid rocket motors are firing at all times. Simulating the jet plumes in a wind tunnel or a computational analysis is difficult and each technique has limitations and shortcomings. Early on in the program, it was believed that CFD simulations would provide the bulk of the data for the aerodynamic database. However, the LAV presented a major challenge because it is a blunt body vehicle flying in a plume-dominated, turbulent flowfield.^{4,5} The CFD simulations required more computational and personnel resources than originally estimated. Although CFD solvers could provide a solution, the CFD solutions had larger than desired uncertainty levels without validation data from a wind tunnel test. The CFD team

spent considerable time developing simulation guidelines for computational analyses of the LAV in order to establish a standard process and also gain confidence in the solutions.^{6,7} The process required stepping through each major component of the powered LAV. This included first modeling the unpowered LAV, then modeling one stand-alone jet plume, then modeling multiple jet plumes, and finally modeling multiple jet plumes in proximity to the vehicle.

On the experimental side, the CAP team also ran into challenges. It was difficult to find test facilities available with the Mach number, Reynolds number, and auxiliary air capabilities necessary for testing of the LAV. Facilities were available to provide the jet plume simulation, but at the cost of lower Reynolds numbers, and vice versa. There was also the difficulty of simulating the jet plumes. Because cold high-pressure air is readily available at wind tunnel facilities, it is commonly used as the simulant gas to model rocket exhaust plumes. However, proper scaling is necessary to account for the differences between the flight plumes and the WT-simulated plumes. Many parameters can be used, and each parameter attempts to capture a different aspect of the plume/flowfield interaction. For most of the wind tunnel tests, it was decided that some combination of nozzle exit Mach number (M_{exit} or $\gamma_{jet} M_{exit}^2$) and thrust coefficient would be the scaling parameters.⁸⁻¹⁰ This allowed the exit pressure ratio and momentum ratio to be matched simultaneously, but not the velocity ratio.

Furthermore, designing one or more air flowpaths in a scale model is challenging. If a flow-through balance is chosen, the flow path design is much simpler, but one of the six balance components would be lost (usually axial force) when the air is flowing. If all six balance components are desired, the flowpath design must include a mechanism for the flowing air to cross the balance from its non-metric end to its metric end. This usually involves high-pressure bellows, which can be difficult to design and fabricate. The bellows need to be strong enough to handle the high pressure and momentum of the flowing air, but also flexible enough to not overwhelm the balance measurements. Given the model scale and mass flow requirements needed for the LAV, this task proved very difficult. The alternative to using an internal strain gauge balance is to instead use a gauged sting to measure forces and moments. This is also difficult to design, and the uncertainty in the measurements could be larger than for an internal balance.

The difficulties encountered in both WT testing and CFD simulations influence the way the aerodynamics can be modeled in the database. This section describes two approaches to modeling the powered aerodynamics of the LAV for the database: incremental aerodynamics and total aerodynamics. The main focus will be on the boost phase portion of the abort sequence, but some material will be presented for the coast, re-orientation, and LAT jettison phases. Figure 3(a) shows a visual illustration of the LAV total aerodynamics model for the boost phase of the abort sequence, while Fig. 3(b) gives the contrasting illustration of the incremental aerodynamics model.

The reference axes and definitions of various quantities for the LAV are given in Fig. 4. For reference, all data in the database is presented on the LAV axis in the LAV aerodynamic coordinate system (Fig. 4(b)) before being rotated 13.3° to the body axis by the API. This axis was chosen to take advantage of the symmetry characteristics of the LAV. Also, all aerodynamic coefficients are presented at the moment reference center (MRC), unless stated otherwise. The MRC for the LAV is located at the theoretical apex of the crew module.

II.A. Incremental Aerodynamics Model

One approach to modeling the aerodynamics of the LAV is to use an incremental method where major effects are isolated and studied separately, then combined by superposition to produce the final result. The major pitfall in this superposition approach is the assumption that each of the effects are separate and independent of each other. This assumption is often not valid for aerodynamics, but if the correlation and coupling between the effects are small, then this approach is at least viable. The advantage to this approach is that it simplifies the requirements for experimental and numerical simulations, giving each technique the best chance for successful results. The CAP team adopted this incremental approach for early versions of the aerodynamic database because of the difficulties in experimental and numerical simulations of the LAV.

Boost Phase

For the boost phase, the effects of the ACM, AM, and vehicle proximity were separated. Figure 3(b) shows the progression from an unpowered vehicle to the total powered vehicle as each incremental effect is added. The choice of model was by necessity, but the CAP team felt the incremental approach could work because

it was believed that the comparatively small ACM jets would have minimal effect on the vehicle because the larger AM jets would dominate the response. The belief was that the ACM effects would be minimal downstream of the upper tower while the AM effects would be on the ogive, which, given its larger surface area and volume, would be a larger factor to vehicle controllability. The team learned later that the ACM and AM effects were more closely coupled because the ACM would change the flowfield upstream of the abort motors enough to affect the location of the AM jet plume boundaries and their proximity to the vehicle, especially in the transonic regime.¹¹

Nonetheless, in the versions of the aerodynamic database that were based on the incremental model, the boost phase database equation¹² is as follows

$$C_{x_{total}} = C_{x_{unpowered}} + \Delta C_{x_{AM}} + \Delta C_{x_{ACM}} + \Delta C_{x_{separation}} \quad (1)$$

where C_x refers to the LAV axis aerodynamic coefficients: C_A, C_N, C_Y, C_m, C_n , and C_l . There is also a dynamic modeling component in this equation that is not shown because it is not pertinent to this discussion. Each of the terms was developed using either WT data or CFD results, and sometimes a mix of the two. Figure 5 shows a graphical representation of how the increments were calculated from the WT and/or CFD data. Since each term came from different data sources, each term also had different uncertainty levels.

For version 0.60 of the database, the AM increment was derived from CFD results designed to characterize the effect of AM C_T and a small thrust offset angle on the LAV (CFD tasks AR-104,¹¹ AR-111, and AR-118¹³). It was calculated by subtracting the integrated forces and moments of the unpowered vehicle from the integrated forces and moments of the powered vehicle. The thrust component of the AM was removed from the powered results by not integrating the AM exit planes. The ACM increment was also derived from CFD results (CFD tasks AR-50¹⁴ and AR-52¹⁵). The increment was also calculated by subtracting unpowered vehicle results from powered vehicle results, but it was done only for the section of the vehicle ahead of the abort motors (upper tower). This was done because it was assumed the effect of the ACM would be most prevalent on the upper tower. Finally, the separation increment was derived from WT results (CAP test 60-AA) that were focused on the effect of AM C_T and axial separation distance (ΔX) on the LAV. The portion of the vehicle from the nose tip to just below the abort motors, including the AM thrust, was on the non-metric end of the balance, and hence, during the WT test, forces exerted on that portion were not measured. This was a consequence of the model design, but the separation effects were assumed to be constrained to the back of the LAV. The effect of the other separation parameters were not examined during the test, but were modeled in the database using either limited CFD results, old Apollo data, or engineering judgment.

Coast and Re-orientation Phases

During the coast and re-orientation phases, the abort motor has burned out and the ACM is the only motor firing for control of vehicle attitude. Development of the coast phase portion of the database is based on two powered ACM wind tunnel tests (CAP tests 75-AA¹⁶ and 76-AA¹⁷), which covered Mach numbers from 0.3 to 4.6, angles of attack from -14° to $+14^\circ$, and angles of sideslip from -10° to $+10^\circ$. The model used a five-component flow-through balance that allowed measurement of all components except axial force when air was flowing, and allowed all components to be measured when air was not flowing. The static ACM thrust was also removed from the final balance data measurements.

The coast phase database equation¹² is shown in Eq. (2), which includes unpowered data and an ACM increment.

$$C_{x_{total}} = C_{x_{unpowered}} + \Delta C_{x_{ACM}} \quad (2)$$

The ACM increment was isolated in the wind tunnel data in order to use symmetry to expand the data set. Figure 6 illustrates how the ACM increment was calculated from the wind tunnel data. Also, a high Reynolds number test of the unpowered LAV (CAP test 83-AA^{18,19}) provided a better set of data from Mach 0.3 to 0.95 for the unpowered term in Eq. (2).

During the re-orientation phase, the LAV travels through higher angles of attack as it is flipped around to a heat shield forward configuration. In the database for this phase, the ACM increment is based solely on CFD data (CFD task AR-108²⁰) with assumptions on ACM firing directions at some re-orientation positions. The unpowered component is also derived from CFD data with some support from WT data (CAP test 27-AD²¹) at angles of attack near 180° .

LAT Jettison Phase

In the LAT jettison phase, the JM fires to move the LAT away from the crew module so that the CM may begin its controlled descent under parachutes. In this separation event, the aerodynamics of the CM is crucial to ensure vehicle stability, but the aerodynamics of the LAT is also important to prevent re-contact between the LAT and the CM after the separation has begun.

Development of the LAT jettison portion of the database is based on three wind tunnel tests (CAP tests 24-AA,^{22,23} 25-AA,^{22,24} and 61-AA²⁵) that simulated the JM jets and the separation effects between the CM and LAT. The tests covered Mach numbers from 0.13 to 2.5, angles of attack from 150° to 190°, and angles of sideslip from -10° to +10°. It also covered various thrust levels of the JM and various longitudinal separation configurations. A balance in the CM model measured CM forces and moments, while a balance in the LAT measured both LAT and CM loads. As a consequence of the model design, the portion of the LAT from the nose tip to just below the jettison motors including the JM thrust was on the non-metric end of the balance, and thus forces on this portion were not measured by the balance.

The database buildup equation¹² for both the CM and LAT during this phase of flight is

$$C_{x_{total}} = C_{x_{unpowered}} + \Delta C_{x_{separation}} \quad (3)$$

The separation increment includes the effect of the JM jets and the proximity effects between the CM and LAT. Similar to the ACM increment, the separation increment was broken out to expand the data set by leveraging symmetry assumptions. Figure 7 illustrates how the separation increment was calculated for the CM and LAT from the wind tunnel data.

II.B. Total Aerodynamics Model

The ultimate goal of the database is to model the complete aerodynamics of the LAV as it travels through each phase of the abort sequence. Thus, a total aerodynamic model is the most desirable approach, since it would simultaneously capture jet interactions between the rocket plumes and the vehicle and capture proximity interactions between separating vehicles. The CAP team had envisioned using this approach from the beginning, but realized early on that both experimental and computational simulations were not mature enough at the time to accomplish the task. It would take a few years to develop the confidence in using both techniques to adequately model the aerodynamics of the LAV.

Boost Phase

Simulating the boost phase in CFD has provided many challenges because of the interactions between two different sets of jet plumes. The jet interactions and corresponding effects on the vehicle are non-linear with respect to the AM thrust coefficient and highly sensitive to small changes in thrust levels of the AM. The problem stems from the varying distance between the AM jet plume boundaries and the vehicle outer mold line (OML).^{11,13} A very dense set of CFD simulations were needed to uncover this nonlinearity and sensitivity. This required a significant amount of time and computing resources, despite the simulations not even accounting for the ACM to AM plume interaction.

On the experimental side, after repeated efforts to build a wind tunnel model capable of simulating the AM and ACM jets simultaneously, the CAP wind tunnel testing team successfully completed such a model and conducted a wind tunnel test of the boost phase LAV in the summer of 2010. The 6%-scale model (Fig. 8) used in CAP wind tunnel test 26-AA contained separate high-pressure air flowpaths for the AM and ACM nozzles, with each flowpath requiring custom-built bellows to be able to bridge the internal strain-gage force balance. The thrust level of the AM and ACM nozzles could be controlled independently during the test. The test covered Mach numbers from 0.3 to 2.5, angles of attack from -14° to +14°, and angles of sideslip from -10° to +10°.

Since both the AM and ACM powered effects were modeled simultaneously, this wind tunnel test provided the data to update the boost phase portion of the LAV aerodynamic database into a total aerodynamic model. Eq. (4) shows the resulting buildup equation¹² for database version 0.61.

$$C_{x_{total}} = C_{x_{boost}} + \Delta C_{x_{separation}} \quad (4)$$

The superposition of the separate unpowered, AM, and ACM effects in Eq. (1) have been replaced by a single term in Eq. (4). The separation effects between the boosting LAV and the launch vehicle stack were

not updated in this database due to a lack of data. Test 26-AA only acquired a small set of vehicle separation data, therefore the separation effects from the previous database were still used.

In the development of the new $C_{x_{boost}}$ term, CFD data were used to provide a WT-to-flight correction to the wind tunnel data. This correction was found to be significant at some conditions and underscores the non-linear nature of the AM plume aerodynamic interaction. The process can be summarized as follows

$$C_{x_{boost}} = \left(WT_{AM} + (\Delta CFD_{AM})_{WT-to-flight} \right) + \Delta WT_{ACM} \quad (5)$$

$$\Delta WT_{ACM} = WT_{AM+ACM} - WT_{AM} \quad (6)$$

$$(\Delta CFD_{AM})_{WT-to-flight} = (CFD_{AM})_{Flight} - (CFD_{AM})_{WT} \quad (7)$$

where the CFD-derived WT-to-flight correction is applied to the powered AM-only wind tunnel data and then the effect of the powered ACM is added. The effect of the powered ACM is obtained by differencing the powered AM-only data from the powered AM+ACM data (Fig. 9).

Also, the CFD-derived WT-to-flight correction is computed by differencing CFD at WT conditions from CFD at flight conditions. The correction not only incorporates scaling to flight Reynolds number, but includes scaling to flight jet plumes (hot gas vs. cold gas), and accounts for differences in geometry between WT models and the flight vehicle. An important distinction between this model and the incremental model presented earlier is that the data increments calculated here come from the same data source.

There are several reasons why the chosen model separates the AM and ACM data, even though the stated goal of the database was to model the aerodynamics of the LAV with both sets of motors firing simultaneously. First, to model the powered AM and ACM together requires five parameters in addition to Mach number and vehicle attitude. Due to time and resource constraints, data were only obtained at a small subset of the total data space. However, by separating the AM and ACM data and by making a few assumptions regarding vehicle symmetry, and by extension, jet interaction symmetry, the dataset can be expanded considerably by reflecting existing ACM data appropriately across symmetry planes. This will be discussed further in a later section. Second, the CFD-derived WT-to-flight correction was computed with the AM firing only. The assumption is that the effect of the ACM on this correction would be minimal and the potential error in this assumption would be covered in the uncertainty buildup.

Coast and Re-orientation Phases

The coast and re-orientation phases were only modeled using an incremental aerodynamics model as discussed in an earlier section.

LAT Jettison Phase

The LAT jettison phase was only modeled using an incremental aerodynamics model as discussed in an earlier section.

II.C. Uncertainty Quantification

Regardless of which modeling approach is taken, the uncertainty in the final database values must be quantified. Uncertainty quantification of the aerodynamic model is dependent on the steps taken in producing a data point in the database table. This takes into account the error in the experimental and numerical simulations in producing the initial data point and the error associated with the process used to transform that initial data point into the final database point. The error construction is different for each modeling approach and multi-dimensional data analysis technique.

For example, as mentioned earlier, the data from CAP wind tunnel test 26-AA were used to update the boost phase portion of the LAV aerodynamic database. With the database buildup process in mind (Eq. (5)), the uncertainty quantification equation was constructed as

$$\begin{aligned} U_{C_x} &= \sqrt{SS} \\ SS &= MI_{WT}^2 \left[2k_{Bal}^2 (u_{C_x})_{Bal}^2 + k_{Rep}^2 (u_{C_x})_{Rep}^2 \right] \\ &\quad + MI_{DBM}^2 \left[k_{ACMsym}^2 (u_{C_x})_{ACMsym}^2 + k_{Interp}^2 (u_{C_x})_{Interp}^2 \right] \\ &\quad + MI_{CFD}^2 \left[2(1 - \rho_{CFD}) k_{CFD}^2 (u_{C_x})_{CFD}^2 \right] \end{aligned} \quad (8)$$

where u_{C_x} quantities are standard deviation estimates of each uncertainty term, k quantities are data coverage factors (≥ 1), and MI quantities are margin index factors (≥ 1). The ρ_{CFD} quantity is a correlation parameter relating the error in CFD at WT conditions to the error in CFD at flight conditions. The uncertainty buildup includes the data uncertainty from the wind tunnel test ($(u_{C_x})_{Bal}$ and $(u_{C_x})_{Rep}$) and any uncertainty or error related to the database modeling steps ($(u_{C_x})_{ACMsym}$, $(u_{C_x})_{Interp}$, and $(u_{C_x})_{CFD}$).

The standard deviation estimates (u_{C_x} quantities) are determined either from calibration results or more frequently, from range analyses of the data (commonly used in statistical process control^{26,27}). The uncertainty coverage factors (k quantities) are determined through inspection of the range analysis results and are chosen to cover approximately 95% (similar to 2σ for a normal distribution) of the residual data. This is frequently set at $\sqrt{3}$ because most of the data tends to exhibit an uniform distribution as opposed to a normal distribution, but the coverage factor can be higher or lower depending on the standard deviation estimate and the residual data. The margin index (MI quantities) can be thought of as bump-up factors to the estimated data uncertainty to cover known errors or deficiencies in the analysis techniques and to cover unknown errors or unmodeled effects. There are separate MI quantities for each block of terms related to wind tunnel data uncertainty, database modeling process uncertainty, and CFD-derived WT-to-flight correction uncertainty. This formulation allowed the CAP team to set each margin index based on the strength and knowledge of the uncertainty analyses of each block.

Error correlation is also investigated when possible (*i.e.*, when enough data is available). To properly propagate errors in database modeling system equations, the correlation of errors between terms in the equation must be known. The common mistake is to assume a conservative stance is achieved by claiming no correlation between errors (*i.e.*, $\rho=0$); in fact, the existence of positive or negative correlation of errors can increase or decrease the overall uncertainty. For example, the strain gauge balance used in the 26-AA wind tunnel test was a force-type balance with two gauges (N_1 and N_2) that are used together to measure normal force and pitching moment (Fig. 10). With the balance moment center at the midpoint between the two gauges, the balance load transformation equations for normal force and pitching moment for this type of balance are shown below

$$NF = N_1 + N_2 \quad (9)$$

$$PM = (N_1 - N_2) \left(\frac{d}{2} \right) \quad (10)$$

where d is the distance between the N_1 and N_2 gauges.

The balance calibration report provided standard deviations of the curve fit error for the N_1 and N_2 gauges (σ_{N_1} and σ_{N_2}). The errors in the NF and PM measurements can be determined by using the load transformation equations (Eqs. 9-10) and the error measures for N_1 and N_2 . The error propagation equations^{28,29} for σ_{NF} and σ_{PM} can be written as

$$\sigma_{NF} = \sqrt{\sigma_{N_1}^2 + \sigma_{N_2}^2 + (2\rho)\sigma_{N_1}\sigma_{N_2}} \quad (11)$$

$$\sigma_{PM} = \sqrt{\sigma_{N_1}^2 \left(\frac{d}{2} \right)^2 + \sigma_{N_2}^2 \left(-\frac{d}{2} \right)^2 + (2\rho)\sigma_{N_1} \left(\frac{d}{2} \right) \sigma_{N_2} \left(-\frac{d}{2} \right)} \quad (12)$$

where ρ is the error correlation parameter between σ_{N_1} and σ_{N_2} . It is clear in Eqs. 11-12 that the existence of error correlation ($\rho \neq 0$) between σ_{N_1} and σ_{N_2} can lead to an increase or decrease in σ_{NF} and σ_{PM} . As it turned out, examination of the N_1 and N_2 residuals from the balance calibration curve fit revealed a strong negative correlation ($\rho \approx -1$) as shown in Fig. 11.

Using this negative correlation parameter in Eq. (11) produced a much lower value for σ_{NF} than what would have resulted had the uncorrelated assumption remained. This contributed to lowering of the overall uncertainty level for normal force. On the flip side, however, using the negative correlation parameter in Eq. (12) increased the value for σ_{PM} . But, with the nature of the root-sum-square, the increase was not as significant as the decrease seen in σ_{NF} .

II.D. Data Comparison of Modeling Approaches

Comparing the boost phase data from two recent versions of the LAV aerodynamic database illustrates the differences between the total aerodynamic model (database version 0.61) and the incremental aerodynamic

model (database version 0.60). Figure 12 shows a comparison of the longitudinal aerodynamic coefficients at Mach 1.1 with the abort motor firing at an AM C_T of 3, and a max ACM firing in the south direction ($\theta_{res} = 180^\circ$). This comparison shows large bias and slope differences in the normal force and pitching moment coefficients between the two databases. The pitching moment slope change was in the negative direction in this example, which may help with vehicle stability, but there are other conditions where the slope change went in the positive direction. Besides the changes in the nominal values, the comparison also shows a large difference in the uncertainty levels for all three coefficients, which has at least as much effect on the GN&C simulations as the changes to the nominal values. Figure 13 shows a comparison of the directional aerodynamic coefficients at Mach 0.9 with the abort motor firing at an AM C_T of 3.5, and a max ACM firing in the east direction ($\theta_{res} = 90^\circ$). This comparison also shows bias differences in the side force and yawing moment coefficients between the two databases and different levels of uncertainty. The size of the database is too large to present comparisons at every possible condition or to make generalizations of the differences. The effect of the differences will be evident in the GN&C simulation failure metrics.

In addition to the differences in the baseline database values, the uncertainty formulation can have a large effect on the final dispersed answer. In the incremental approach for the boost phase, the equation for computing a dispersed aerodynamic coefficient is as follows

$$\begin{aligned}
C_{x_{dispersed}} &= C_{x_{unpowered}} + \epsilon_{unpowered} U_{C_{x_{unpowered}}} \\
&\quad + \Delta C_{x_{AM}} + \epsilon_{AM} U_{C_{x_{AM}}} \\
&\quad + \Delta C_{x_{ACM}} + \epsilon_{ACM} U_{C_{x_{ACM}}} \\
&\quad + \Delta C_{x_{separation}} + \epsilon_{separation} U_{C_{x_{separation}}}
\end{aligned} \tag{13}$$

where the ϵ quantities are randomly drawn between -1 and 1 from a uniform distribution and the U_{C_x} quantities are the total uncertainty values for the aerodynamic coefficients. Each of the terms came from different data sources (*i.e.*, different wind tunnel tests or CFD results) and hence have different uncertainty levels. One limitation with this approach is that it is very difficult in practice to determine the possible correlation between each of these terms. As discussed earlier, without this information, the total uncertainty level could be unnecessarily large or could be too small. Another fear is the possibility of accounting for an error source multiple times (*i.e.*, double-counting) in this process. A consequence of Eq. (13) is that the superposition of multiple uniform distributions results in a trapezoidal distribution. This means that the GN&C simulations have less chance of drawing the largest uncertainty level from each term (worst-on-worst). This was not obvious to the CAP team at first, but this realization changed how the simulation results were viewed.

For the total aerodynamic model for the boost phase, the equation for computing a dispersed aerodynamic coefficient is

$$\begin{aligned}
C_{x_{dispersed}} &= C_{x_{boost}} + \epsilon_{boost} U_{C_{x_{boost}}} \\
&\quad + \Delta C_{x_{separation}} + \epsilon_{separation} U_{C_{x_{separation}}}
\end{aligned} \tag{14}$$

The main difference between Eq. (13) and Eq. (14) is that the six terms related to the unpowered, AM, and ACM effects have been replaced by just two terms related to the combined AM and ACM effect. This also eliminates the superposition of three uniform distributions.

Figure 14 shows a comparison of the histograms for 2,000 random drawings of database uncertainty for pitching moment coefficient and axial force coefficient between two recent versions of the database. Database version 0.60 had the incremental aerodynamics approach as exemplified in Eq. (13) while database version 0.61 switched over to the total aerodynamics approach discussed in Eq. (14). The comparison shows the difference between adding up uniform distributions for the separate unpowered, AM, and ACM uncertainties in version 0.60 (notice the trapezoidal distribution) and the uniform distribution for the combined AM and ACM uncertainty of version 0.61. Also, the magnitude of the maximum uncertainty levels between the two databases is different. For the total aerodynamics approach in version 0.61, the data came mainly from one source (wind tunnel test 26-AA), which simplified the uncertainty model. For example, the axial force measurements from the test were very accurate and repeatable, and the effects of that accuracy can be seen in the uncertainty result as compared to version 0.60.

III. Complexities of Multi-Dimensional Data

Modeling the aerodynamics of the LAV requires a large multi-dimensional data space, which introduces a set of potential problems. The correct independent parameters must be determined to accurately describe the model, however, the data space quickly grows with each added dimension. It is nearly impossible to fill in all areas of the data space, especially with the time and resource constraints attached to any experimental or numerical simulation. This section describes the problems encountered by the CAP team in working with multi-dimensional data and includes examples of solutions adopted by the database developers.

III.A. Parameterization

Since the data space can grow rapidly, it is important to determine the best parameters to describe the model and avoid adding extraneous parameters. The chosen parameters must be unique, well-defined, and easily measurable. Sometimes, when there are many candidate parameters to describe a model, it is possible to combine them, resulting in fewer parameters to describe the model.

An example of this is with the attitude control motor. Recall that the ACM is a solid rocket motor fired through eight variable-thrust, circumferential nozzles (Fig. 15). The nozzles are designated N1 through N8 with N1 at an azimuth angle of 22.5° from the top and the others following at 45° increments. Because of the circumferential nature of the thrust profiles, the ACM has a large number of firing combinations. A thrust allocation algorithm is used to define the individual nozzle thrusts required to obtain a specified overall thrust level and direction. Figure 16 shows some of the ACM thrust allocation profiles.

The database team was able to describe all of the possible ACM firing combinations with only three parameters: resultant firing direction, thrust coefficient, and thrust balance. However, this three-parameter set is only valid given the current ACM thrust allocation algorithm and an assumed nominal engine performance level. Off-nominal engine performance is accounted for in increased uncertainty levels.

The first parameter is the resultant firing direction, which is simply the vector resultant of the individual nozzle force vectors. The resultant thrust direction is sometimes used and this is defined as being in the opposite direction of the resultant firing direction

$$\theta_{thrust} = 180 - \theta_{res} \quad (15)$$

Thrust coefficient is defined as total thrust non-dimensionalized by freestream dynamic pressure and vehicle reference area. For the ACM, the thrust from each nozzle is resolved along the resultant thrust vector and then summed. In the current thrust allocation algorithm, the thrust components perpendicular to the resultant thrust vector cancel out by design. The total thrust coefficient is then defined as

$$C_{T_{ACM}} = \frac{\sum_{i=1}^8 F_i |\cos(\theta_i - \theta_{res})|}{q_\infty S_{ref}} \quad (16)$$

The thrust balance is defined as the ratio of a) thrust only in the direction of the resultant thrust to b) the total thrust aligned along the thrust vector (thrust in either direction along the thrust vector)

$$T_{bal_{ACM}} = \frac{\sum_{i=1}^8 F_i \cos(\theta_i - \theta_{res})}{q_\infty S_{ref} C_{T_{ACM}}} \quad \text{for } 0 \leq \cos(\theta_i - \theta_{res}) \leq 1 \quad (17)$$

The thrust balance parameter is needed because the ACM cannot operate with all of its nozzles closed simultaneously due to overpressurization of the motor plenum. Therefore, to produce a zero resultant thrust, it must command a directional null thrust profile, where thrust on one side of the tower is counter-balanced with thrust on the opposite side. In the ACM thrust allocations, the thrust balance number can be between 0.5 (null thrust) and 1 (max thrust). Figure 17 shows definitions of the thrust vector quantities used in Eqs. (16) and (17).

Vehicle separation is another example that showcases the large number of independent parameters required in the database. During the boost phase and LAT jettison phase, two vehicles are separating from each other. In addition to the jet thrust parameters for the AM or JM, the position of the vehicles relative

to each other must be known in order to correctly describe the proximity aerodynamics present in these scenarios. This includes translational separation distances in 3-dimensions (ΔX , ΔY , ΔZ) and differences in the vehicle rotational angles ($\Delta\alpha$, $\Delta\beta$). Figure 18 shows the separation parameter definitions for the LAV separation from the launch stack and for the CM separation from the LAT. In wind tunnel tests, it is difficult to design a model to be able to vary each of these parameters independently. Understandably, only a subset of the parameters can be varied, typically the parameters in the longitudinal plane are especially important for vehicle control. Figure 19 shows examples of vehicle separation mechanisms in CAP wind tunnel tests that were designed to allow independent variation of the longitudinal separation parameters (ΔX , ΔZ , $\Delta\alpha$).

III.B. Response Surface Methods

The experimental and numerical simulations produce a finite set of data points within the multi-dimensional data space. Time, resource, and various other constraints prevent obtaining data points at every possible combination of independent parameters. Careful planning and prioritizing before an experimental or numerical simulation helps to select the most important data points to obtain. In addition, it is sometimes important to pick data points at corners of the data space in order to avoid extrapolation.

As a result, multi-dimensional response surface methods have been utilized in the development of the Orion aerodynamic database. Figure 20 shows an example of a response surface for the coast phase ACM pitching moment coefficient increment. The response surface methods are sometimes used simply to produce data at cardinal setpoints from an input set of experimental data. Other times, they are used to fill in areas that were not addressed in the simulations by interpolating within the input data set. This comes with an additional uncertainty, which can vary depending on the distance the interpolated point is from any input data points.

One of the response surface tools used in the Orion database development has been the Kriging response surface. It belongs to the family of linear least squares estimation algorithms and seeks to perform optimal interpolation based on regression against observed values of surrounding data points, weighted according to spatial covariance values.³⁰⁻³² A Matlab toolbox is available that implements the Kriging algorithm^{33,34} and allows the choice of underlying regressor as well as a choice of correlation models. It was chosen for database development because it can handle multiple dimensions of data, it has flexibility in tuning of response surface details, and it provides an estimated interpolation error. The technique works well with data that are fairly dense and uniformly distributed in all dimensions. When this was not the case, the data needed to be split into subsets to avoid the pitfalls of the technique.

An example where the data needed to be split into subsets is with the development of the LAT jettison portion of the database. Because of the proximity effects between the CM and LAT and the jet interaction effects of the JM, this data space would need nine dimensions (Mach, α , β , JM C_T , ΔX , ΔY , ΔZ , $\Delta\alpha$, $\Delta\beta$) to fully describe it. CAP wind tunnel test 24-AA was not able to investigate the effect of ΔY or $\Delta\beta$, so the resulting database was a seven degrees of freedom (DOF) database. The wind tunnel test could not test all possible combinations of ΔX , ΔZ , and $\Delta\alpha$, so the response surface was relied upon to produce this data (Fig. 21). However, with 7-DOF, the amount of data was overwhelming to the Kriging tool. Therefore, the data were split into “zones” by Mach number and angle of attack because those two dimensions were the most dense. The other dimensions were held intact. Each zone overlapped with a neighboring zone by at least one Mach number and one angle of attack setpoint (Fig. 22). The zones were then treated as separate response surfaces and run through the Kriging tool. Finally, each separate zone was patched together to produce the final response surface (Fig. 23) where the overlapping portions were averaged.

III.C. Extending Data Across the Data Space

The data tables in the Orion aerodynamic database are required to be “square”, meaning that there must be a data value at every combination of the independent parameter values. This is a consequence of the original database design. Inevitably, there are always areas of the data space that have not been covered by the experimental or numerical simulations or filled in by a response surface. In order to fill in these areas, additional information is used, such as trending information from neighboring points or vehicle symmetry assumptions that can be leveraged.

In the LAV aerodynamic coordinate system (Fig. 4(b)), the vehicle is nearly axisymmetric with a few OML features, such as the tower raceway and the umbilical cutout in the ogive, that prevent total symmetry. However, the effects of those features are small, and the database developers have used symmetry assumptions

to fill in untested areas of the data space with reflected data. Doing this does not come without a penalty, though. Some extra uncertainty is added for leveraging vehicle symmetry, usually through analysis of wind tunnel or CFD data that seeks to test the validity of the assumption.

An example where the vehicle symmetry assumption is used in the development of the LAV database is with the coast phase ACM jet interaction increments (Eq. (2)). In wind tunnel tests of the coast phase looking at ACM jet interaction effects, only a limited set of ACM firing combinations were tested. These were chosen carefully with the knowledge that symmetry would be used to fill in data for untested firing combinations. This helped to keep the test matrix within resource constraints. Figure 24 summarizes the ACM firing directions that were either tested or covered using symmetry. The firing directions tested lay in quadrant 4 and cover east to south firings. Figure 25 presents the equations used to reflect ACM jet interaction increment data from firing directions in quadrant 4 to firing directions in the other three quadrants. It is important to note that reflecting data as such states that the ACM jet interaction aerodynamic increment data is symmetric, and not just the vehicle. When data is reflected, special consideration must be made regarding conditions at the boundaries of the reflection plane. Data inflections or asymptotic jumps in the data can occur at the boundaries. To prevent this, a set of symmetry “rules” for the ACM jet interaction increment data were created and are shown in Fig. 26.

Examples showing the application of the symmetry rules are shown in Fig. 27. For a max south ACM firing, the yawing moment coefficient needs to be symmetric about $\beta=0^\circ$. As shown in Fig. 27(a), the original WT data is pretty close to being symmetric. The symmetry rule is applied by finding the average magnitude of the yawing moment coefficient between the positive and negative sideslip data, then reflecting the result to the opposite sign. Similar examples are shown for pitching moment coefficient for a max east ACM firing and for side force coefficient for a null south ACM firing.

The CM and LAT separation increment data (Eq. (3)) during the LAT jettison phase provides another example where the vehicle symmetry assumption is used. In this case, there are a few features that violate the assumption. For the LAT, in addition to the small OML details mentioned earlier, the jettison motor plumes are also not symmetric because one nozzle has a smaller throat than the other nozzles. For the CM, various OML details such as windows and doors prevent complete axis symmetry. In the wind tunnel test, an angle of attack range between 150° and 190° was acquired. Also, only negative Z-separation distances ($-\Delta Z$) and positive relative angle of attack differences ($+\Delta\alpha$) were tested. To fill in up to 210° angle of attack and to fill in for positive Z-separation distances and negative relative angle of attack differences, the separation increment data were reflected about the $\alpha=180^\circ$, $\Delta Z=0$, and $\Delta\alpha=0$ point (Fig. 28). Figure 29 shows the reflection equations for this scenario.

An example showing the reflection of separation increment data for the crew module is shown in Fig. 30. The original pitching moment coefficient data is from a configuration with $\Delta Z = -0.2$ and $\Delta\alpha = +6^\circ$. To get the data for the reflected configuration ($\Delta Z = +0.2$ and $\Delta\alpha = -6^\circ$), the original pitching moment coefficient data is first mirrored across $\alpha = 180^\circ$, then the sign is reversed on the result to produce the final data curve.

IV. Concluding Remarks

The Orion CAP team has overcome many challenges in modeling the aerodynamics of the LAV for the aerodynamic database. Wind tunnel and CFD techniques for simulating powered aerodynamics of the LAV were not mature enough early in the project, but gained major improvements during the development process as the LAV progressed through several design cycles. Two powered aerodynamics modeling approaches were presented: one involved an incremental approach where multiple powered jet effects were investigated separately and the results were combined by superposition, and the other was a total aerodynamics approach where all powered jet effects were investigated simultaneously as a whole. Comparisons between the two approaches were made including database comparisons of nominal and uncertainty values for the boost phase of the launch abort sequence. Finally, examples were presented detailing the methods used by the database developers to tackle the difficulties of a large multi-dimensional data space needed for the LAV. These include intelligent parametrization of the data space, use of advanced response surface methods, and methods for extending data across the data space such as leveraging vehicle symmetry.

Acknowledgments

The authors would like to acknowledge the hard work and dedication of the Orion CAP team in development of the LAV aerodynamic database. The wind tunnel and CFD groups took major steps in improving the state of the art for powered aerodynamic simulations for vehicles such as the LAV and their efforts produced quality data for use in the database. The database and uncertainty groups also worked to improve modeling and uncertainty quantification methods to ensure the highest quality database and ease of use for end-users.

References

- ¹NASA, "http://www.nasa.gov/mission_pages/constellation/orion/," .
- ²Robinson, P. E. and Wilson, T. M., "Orion Aerodynamic Databook, Ver 0.61," NASA CXP-72167, Mar. 2011.
- ³A.Thompson, J., "CEV Aerodynamic Database Application Programming Interface User's Guide," CEV Aerosciences Project, Rept. EG-CAP-09-138, NASA Johnson Space Center, Houston, TX, March 2011.
- ⁴Rogers, S. E. and Pulliam, T. H., "Computational Challenges in Simulating Powered Flight of the Orion Launch Abort Vehicle," 29th AIAA Applied Aerodynamics Conference, Honolulu, HI, 27-30 June 2011 (submitted for publication), American Institute of Aeronautics and Astronautics, Reston, VA.
- ⁵Shestopalov, A. J., Childs, R. E., and Melton, J. E., "Turbulence Model Assessment for Hot Plumes," 29th AIAA Applied Aerodynamics Conference, Honolulu, HI, 27-30 June 2011 (submitted for publication), American Institute of Aeronautics and Astronautics, Reston, VA.
- ⁶Childs, R. E., Garcia, J. A., Melton, J. E., Rogers, S. E., Shestopalov, A. J., and Vicker, D. J., "Overflow Simulation Guidelines for Orion Launch Abort Vehicle Aerodynamic Analyses," 29th AIAA Applied Aerodynamics Conference, Honolulu, HI, 27-30 June 2011 (submitted for publication), American Institute of Aeronautics and Astronautics, Reston, VA.
- ⁷Rogers, S. E., Olsen, M. E., Childs, R. E., Manning, T. A., Garcia, J. A., and Vicker, D. J., "LAV CFD Simulation Guidelines for the OVERFLOW 2 Navier-Stokes Solver," CEV Aerosciences Project, Rept. EG-CAP-10-06, NASA Ames Research Center, Moffett Field, CA, 2010.
- ⁸Brauckmann, G. J., Greathouse, J. S., and White, M. E., "Rocket Plume Scaling for Orion Wind Tunnel Testing," 29th AIAA Applied Aerodynamics Conference, Honolulu, HI, 27-30 June 2011 (submitted for publication), American Institute of Aeronautics and Astronautics, Reston, VA.
- ⁹Brauckmann, G. J., "Abort Motor Nozzle Scaling for Test 26-AA," CEV Aerosciences Project, Rept. EG-CAP-11-04, NASA Langley Research Center, Hampton, VA, 2011.
- ¹⁰Brauckmann, G. J., "Attitude Control Motor Nozzle Scaling for Test 59-AA," CEV Aerosciences Project, Rept. EG-CAP-10-101, NASA Langley Research Center, Hampton, VA, Sept. 2010.
- ¹¹Vicker, D., "OVERFLOW Analysis of AM Thrust Offset and ACM/AM Interaction Effects," CEV Aerosciences Project, Rept. EG-CAP-09-84, NASA Johnson Space Center, Houston, TX, Nov. 2009.
- ¹²Robinson, P. E. and A.Thompson, J., "Formulation of the Orion Aerodynamic Database," CEV Aerosciences Project, Rept. EG-CEV-06-37, NASA Johnson Space Center, Houston, TX, Mar. 2011.
- ¹³Vicker, D., "OVERFLOW Analysis of AM Thrust Offset Effects Part 2 and 3," CEV Aerosciences Project, Rept. EG-CAP-10-73, NASA Johnson Space Center, Houston, TX, Jul. 2010.
- ¹⁴Aftosmis, M. J. and McMullin, M., "LAV-068 ACM Assessment using Cart3D," CEV Aerosciences Project, Rept. EG-CAP-07-107, NASA Ames Research Center, Moffett Field, CA, Aug. 2007.
- ¹⁵Rogers, S., "LAV-068 ACM Assessment using OVERFLOW," CEV Aerosciences Project, Rept. EG-CAP-07-89, NASA Johnson Space Center, Houston, TX, Jul. 2007.
- ¹⁶Murphy, K. J., Brauckmann, G. J., Chan, D. T., Walker, E. L., Mayfield, D., and Cross, J., "Final Report for Test 75-AA - Attitude Control Motor Jet Interaction Testing of ALAS-11 Rev. 3c in the Ames Unitary Plan Wind Tunnel," CEV Aerosciences Project, Rept. EG-CAP-10-87, NASA Langley Research Center, Hampton, VA, 2011.
- ¹⁷Paschal, K. B., Murphy, K. J., Chan, D. T., Brauckmann, G. J., Fuchs, A., Mayfield, D., and Cross, J., "Attitude Control Motor Jet-Interaction Testing of the ALAS-11-Rev3c LAV in the Langley Unitary Plan Wind Tunnel," CEV Aerosciences Project, Rept. EG-CAP-10-90, NASA Langley Research Center, Hampton, VA, 2011.
- ¹⁸Chan, D. T. and Brauckmann, G. J., "Flight Reynolds Number Testing of the Orion Launch Abort Vehicle in the NASA Langley National Transonic Facility (Invited)," 29th AIAA Applied Aerodynamics Conference, Honolulu, HI, 27-30 June 2011 (submitted for publication), American Institute of Aeronautics and Astronautics, Reston, VA.
- ¹⁹Chan, D. T., Brauckmann, G. J., and Walker, E. L., "Final Report for Test 83-AA - High Reynolds Number Test of the Unpowered Launch Abort Vehicle in the NASA LaRC National Transonic Facility," CEV Aerosciences Project, Rept. EG-CAP-09-54, NASA Langley Research Center, Hampton, VA, May 2009.
- ²⁰Schwing, A., "OVERFLOW Analysis of High Alpha ACM Analysis," CEV Aerosciences Project, Rept. EG-CAP-10-46, NASA Johnson Space Center, Houston, TX, Nov. 2009.
- ²¹Owens, B., "27-AD Subsonic-Transonic Launch Abort Vehicle Dynamic Stability Test in the NASA LaRC Transonic Dynamics Tunnel," CEV Aerosciences Project, Rept. EG-CAP-08-79, NASA Langley Research Center, Hampton, VA, 2008.
- ²²Rhode, M. N., Chan, D. T., Niskey, C. J., and Wilson, T. M., "Aerodynamic Testing of the Orion Launch Abort Tower Separation with Jettison Motor Jet Interactions," 29th AIAA Applied Aerodynamics Conference, Honolulu, HI, 27-30 June 2011 (submitted for publication), American Institute of Aeronautics and Astronautics, Reston, VA.
- ²³Rhode, M. N., "CAP Wind Tunnel Test 24-AA Final Report," CEV Aerosciences Project, Rept. EG-CAP-10-89, NASA Langley Research Center, Hampton, VA, 2011.

²⁴Niskey, C. J., "CAP Wind Tunnel Test 25-AA Final Report," CEV Aerosciences Project, Rept. EG-CAP-10-88, NASA Langley Research Center, Hampton, VA, 2011.

²⁵Wilson, T. M., "61-AA LAS Jettison Motor and Proximity Wind Tunnel Test for PA-1 and ALAS 11 Rev3c at the Langley 14x22 Facility," CEV Aerosciences Project, Rept. EG-CAP-09-05, NASA Johnson Space Center, Houston, TX, Mar. 2009.

²⁶Wheeler, D. and Chambers, D., *Understanding Statistical Process Control*, SPC Press, Knoxville, 2nd ed., 1992.

²⁷Wheeler, D., *Advanced Topics in Statistical Process Control*, SPC Press, Knoxville, 1995.

²⁸"U.S. Guide to the Expression of Uncertainty in Measurement," Tech. Rep. ANSI/NCSL Z540-2-1997, October 1997.

²⁹Bevington, P. R. and Robinson, D. K., *Data Reduction and Error Analysis for the Physical Sciences*, McGraw-Hill, 3rd ed., 2002.

³⁰Chiles, J.-P. and Delfiner, P., *Geostatistics, Modeling Spatial Uncertainty*, Probability and Statistics, Wiley, 1999.

³¹Cressie, N., *Statistics for spatial data*, Wiley, New York, 1993.

³²Sacks, J., Welch, W. J., Mitchell, T. J., and Wynn, H. P., "Design and Analysis of Computer Experiments," *Statistical Science*, Vol. 4, No. 4, 1989, pp. 409–435.

³³Lophaven, S. N., Nielsen, H. B., and Sondergaard, J., "DACE - A Matlab Kriging Toolbox," Informatics and Mathematical Modeling, Rept. IMM-TR-2002-12, Technical University of Denmark, Aug. 2002.

³⁴Lophaven, S. N., Nielsen, H. B., and Sondergaard, J., "Aspects of the Matlab Toolbox DACE," Informatics and Mathematical Modeling, Rept. IMM-REP-2002-13, Technical University of Denmark, 2002.

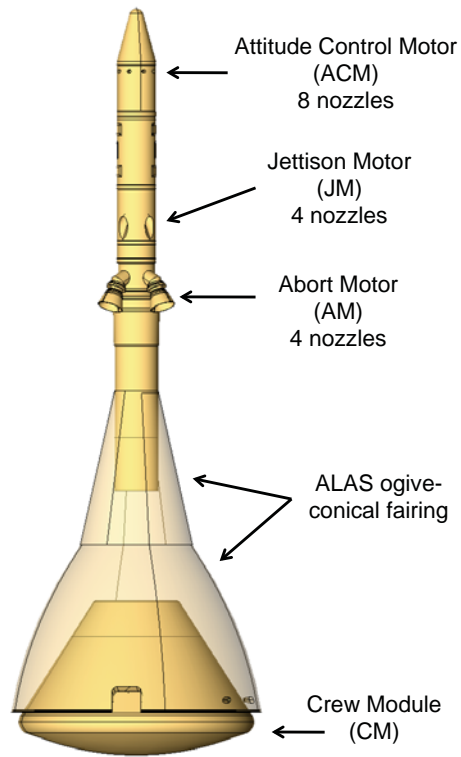


Figure 1. Orion Launch Abort Vehicle.

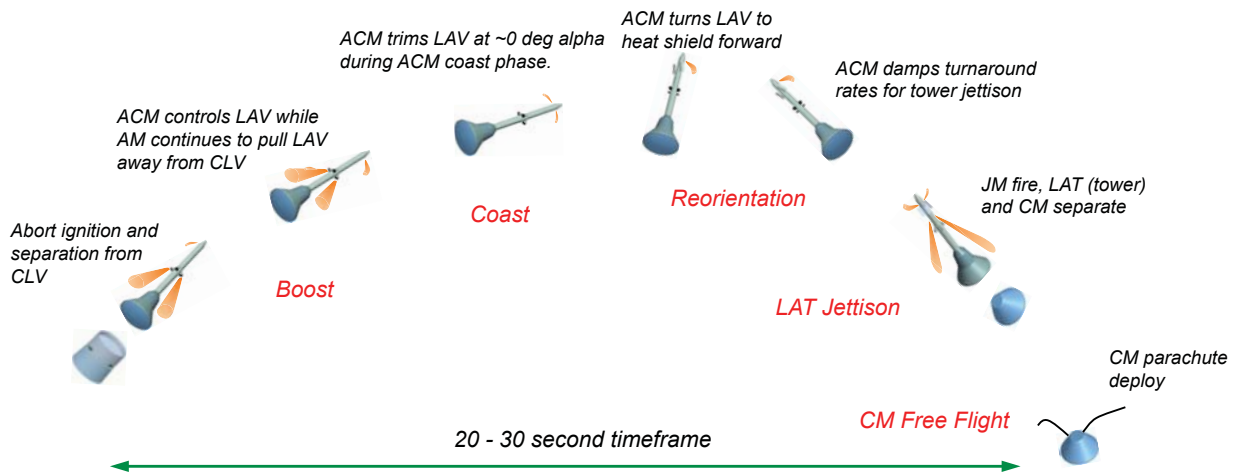
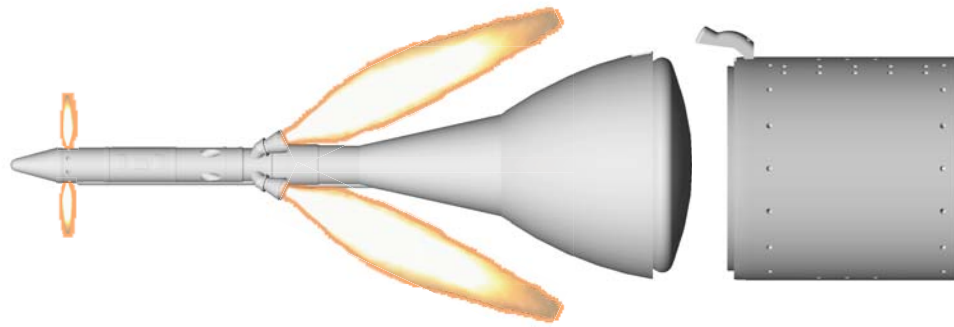
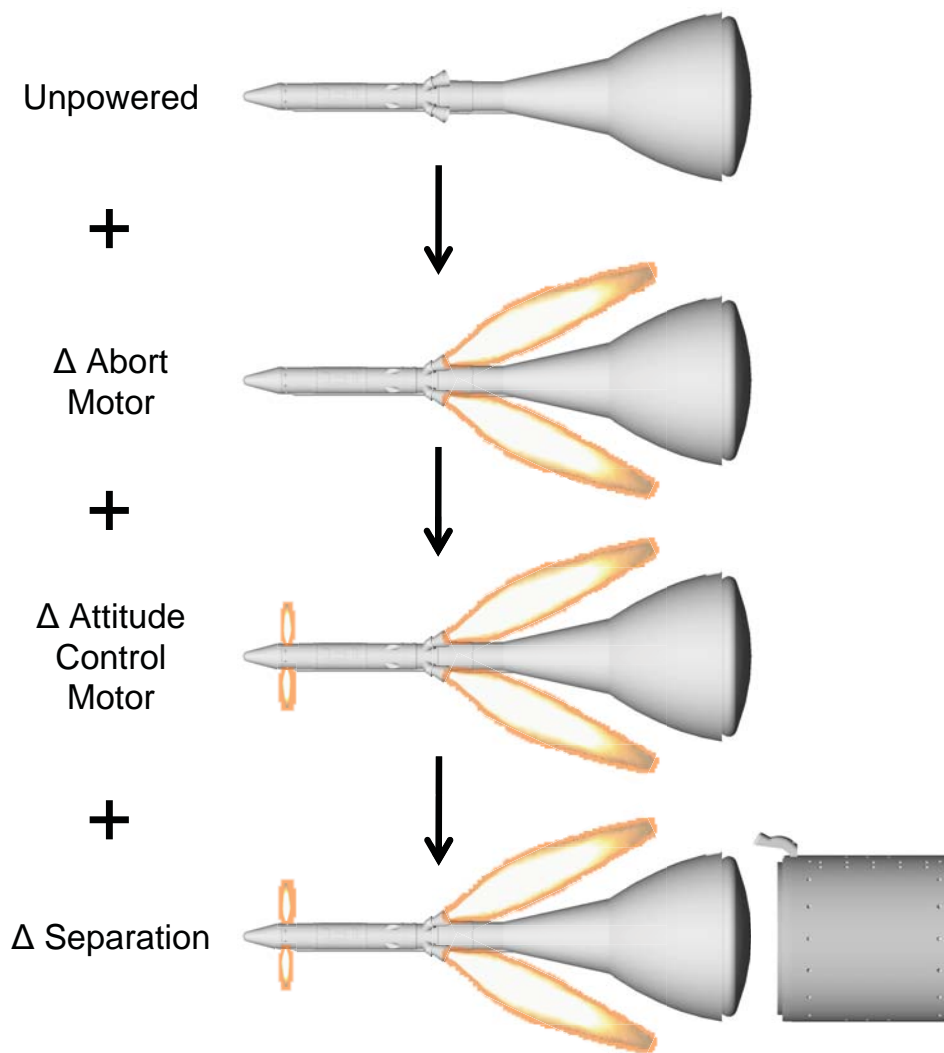


Figure 2. Phases of LAV abort sequence.

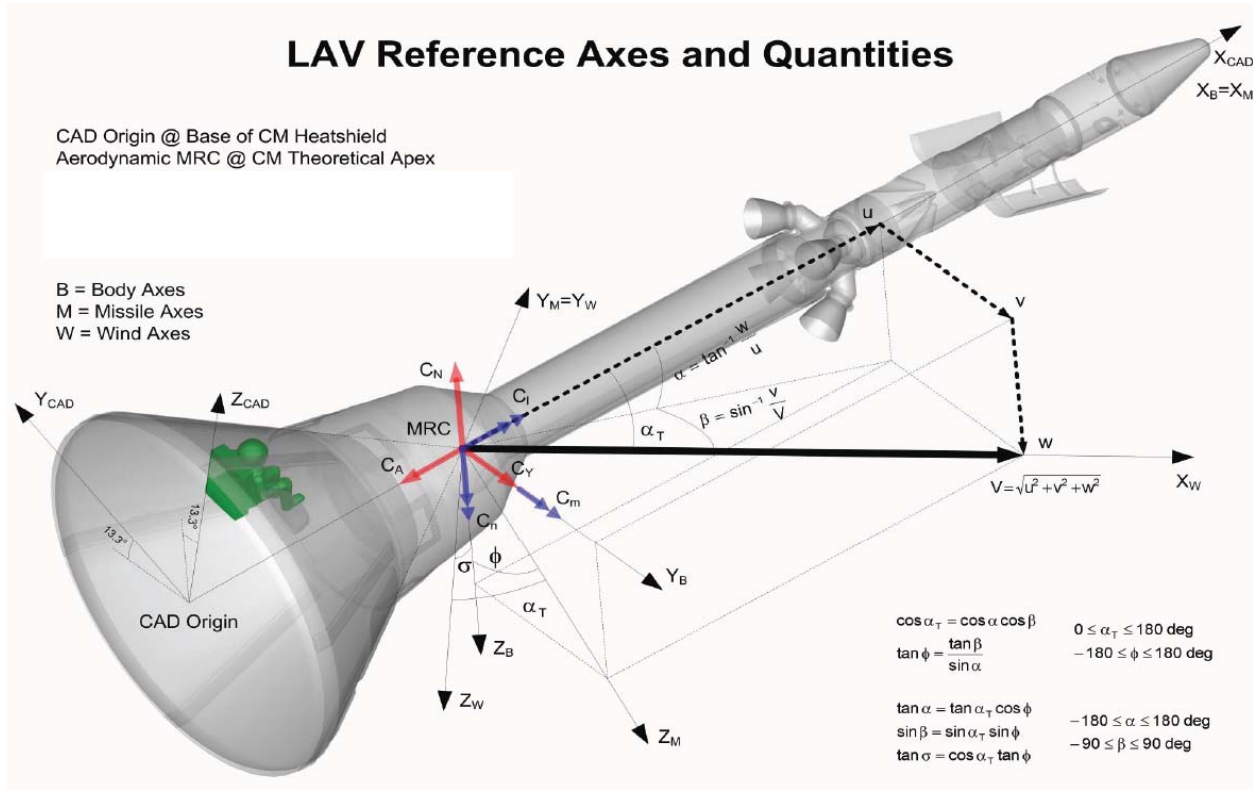


(a) Total Aero Model

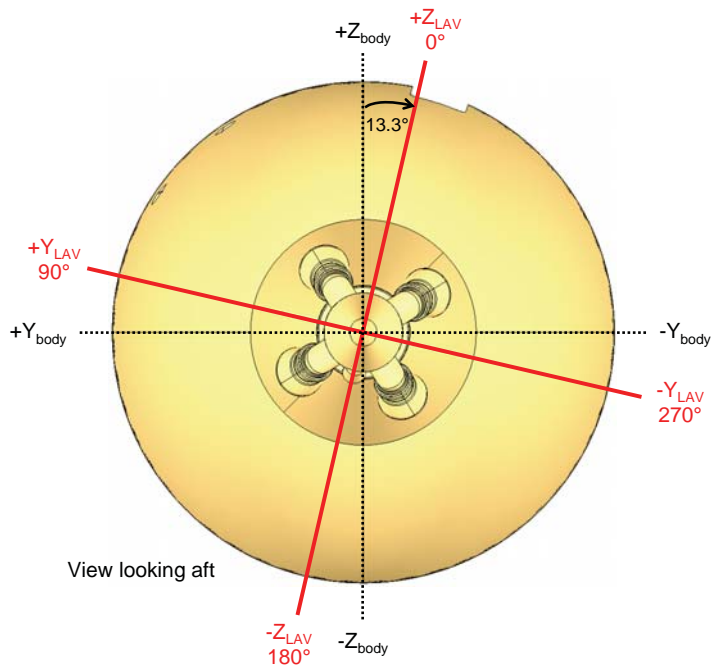


(b) Increment Aero Model

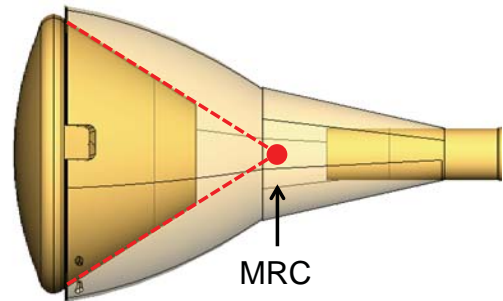
Figure 3. Comparison between LAV boost phase aerodynamic database modeling approaches.



(a) Axes system definitions and sign conventions



(b) LAV aerodynamic coordinate system



(c) Moment Reference Center (MRC) location

Figure 4. LAV axes system and definitions.

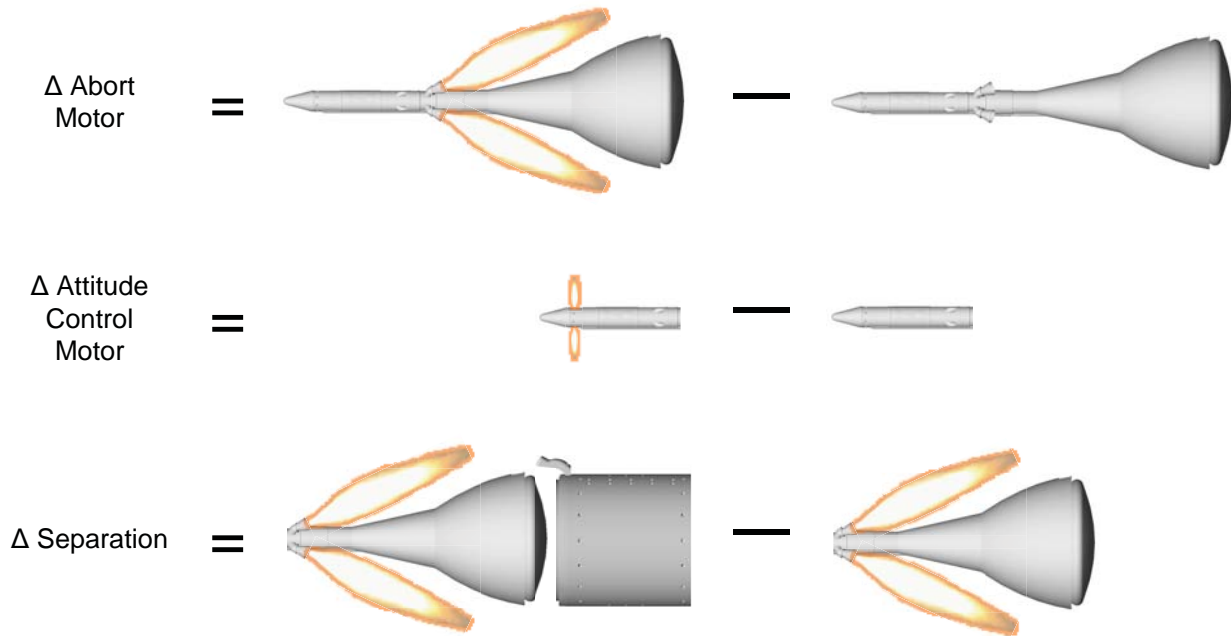


Figure 5. Illustration showing how the increment data in Eq. (1) were derived from WT and/or CFD data.

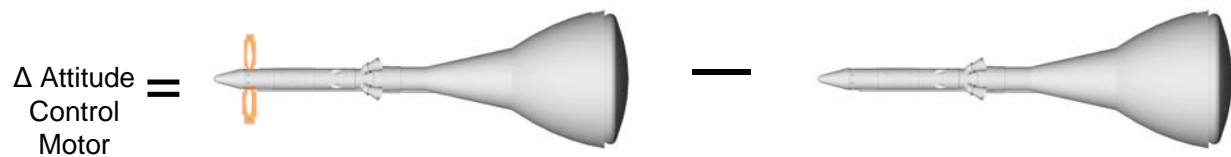


Figure 6. Illustration showing how the ACM increment data (Eq. (2)) was derived in CAP Tests 75-AA and 76-AA.

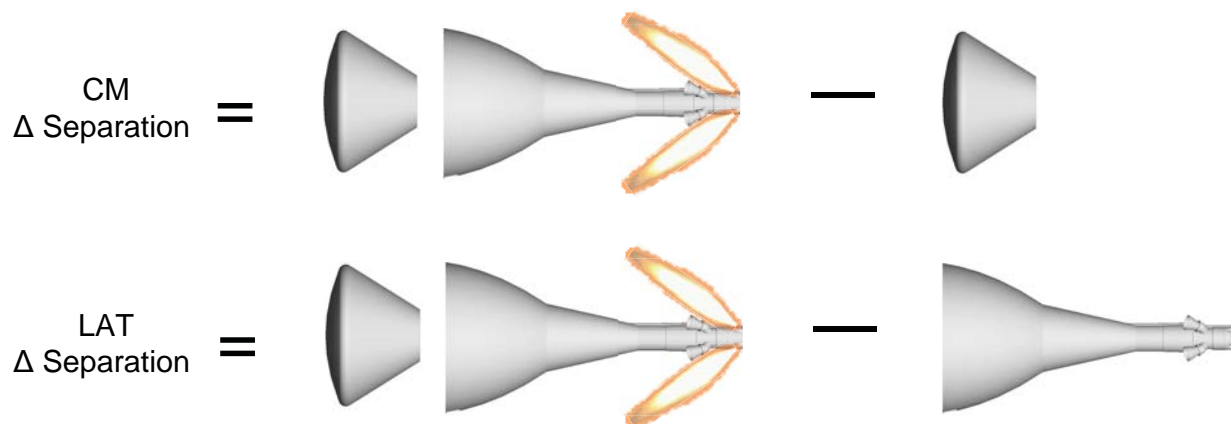
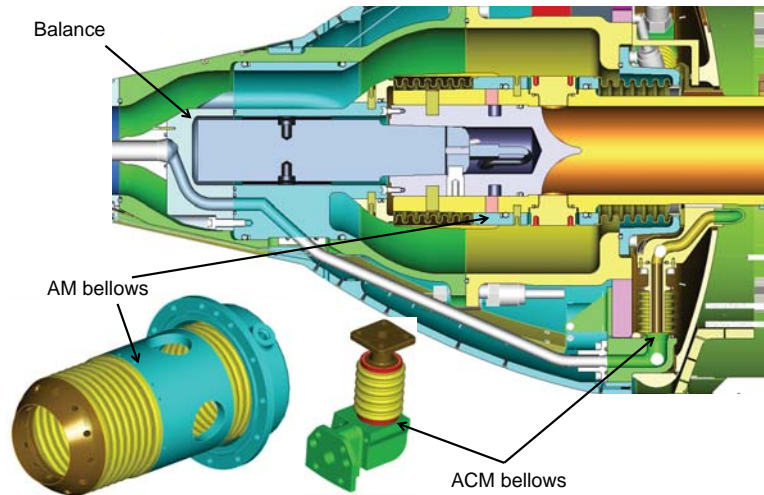


Figure 7. Illustration showing how the separation increment data (Eq. (3)) was derived in CAP Tests 24-AA, 25-AA, and 61-AA.



(a) Photo of model in NASA Ames Unitary Wind Tunnel



(b) AM and ACM flowpath bellows

Figure 8. 6%-scale wind tunnel model of the LAV used in CAP Test 26-AA.

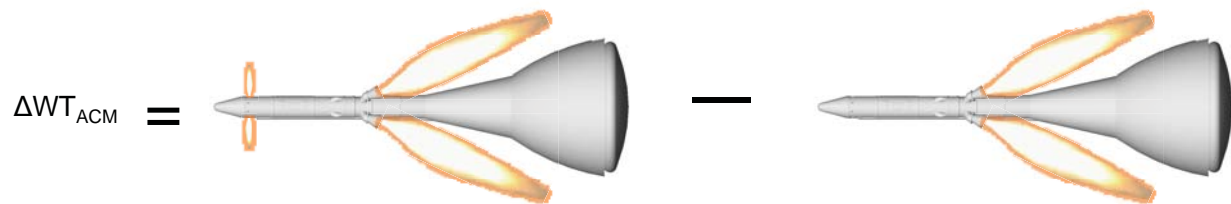


Figure 9. Illustration showing how the ACM increment data (Eq. (6)) was derived in CAP Test 26-AA.

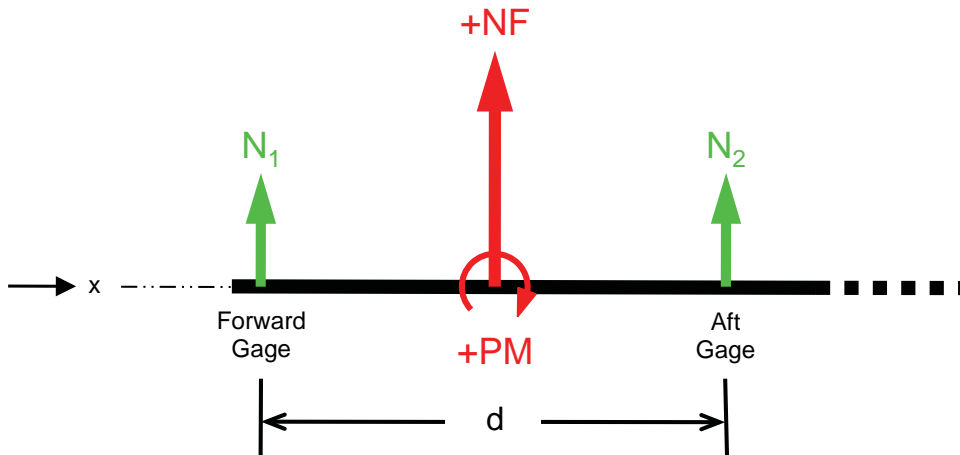


Figure 10. Example free-body force diagram for a force-type strain gauge balance.

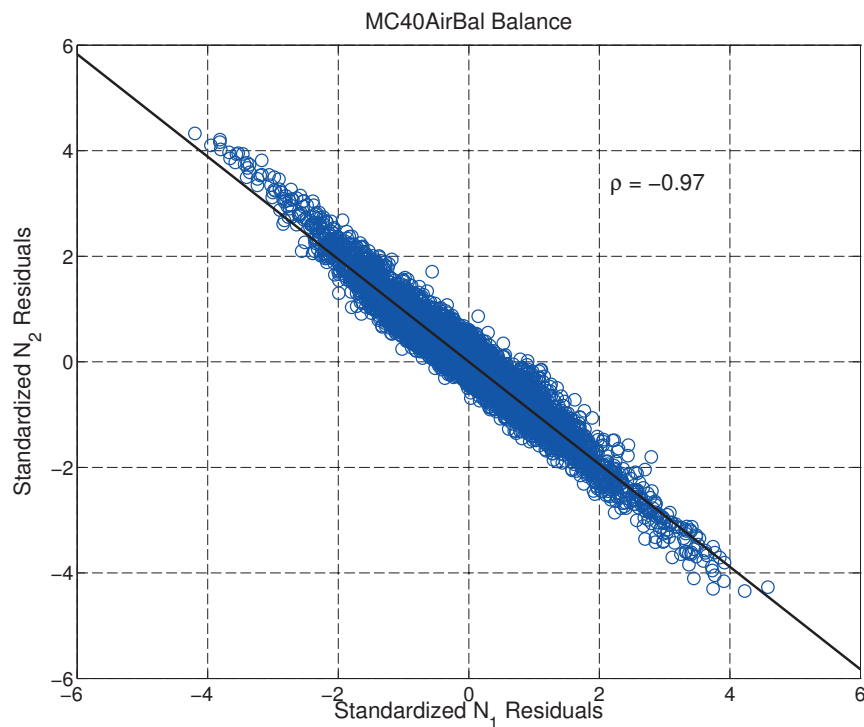


Figure 11. Strong negative correlation seen between N_1 and N_2 residuals from the balance calibration curve fit.

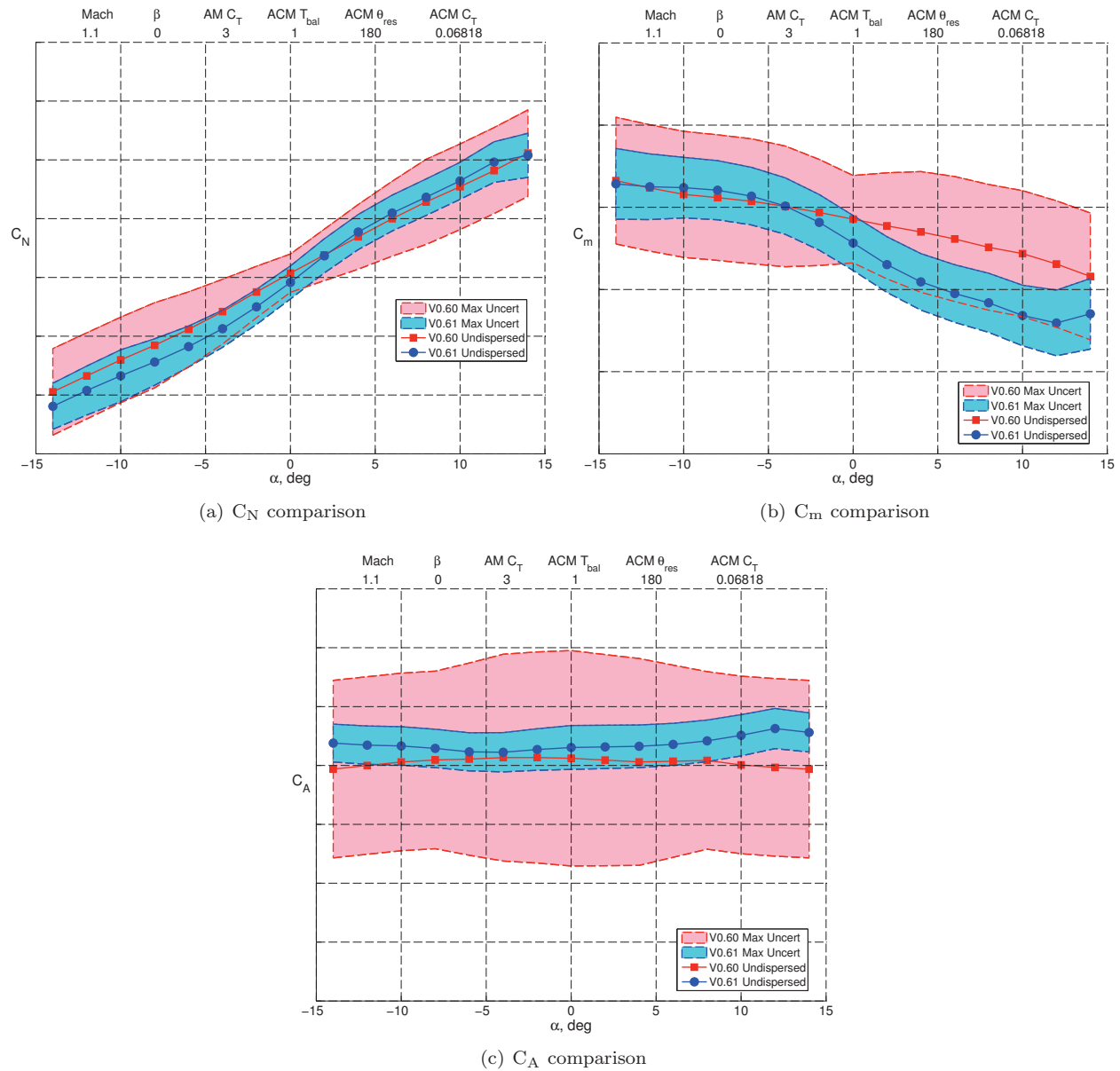


Figure 12. Comparison of longitudinal aerodynamic coefficients between database version 0.60 (increment aero) and version 0.61 (total aero).

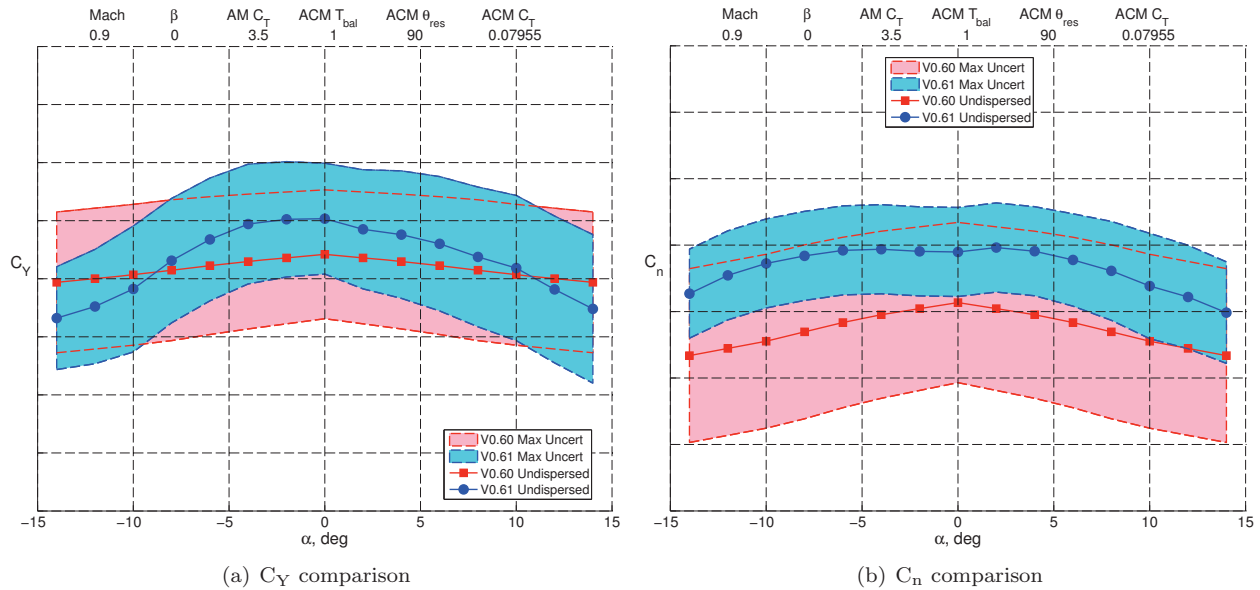


Figure 13. Comparison of lateral aerodynamic coefficients between database version 0.60 (increment aero) and version 0.61 (total aero).

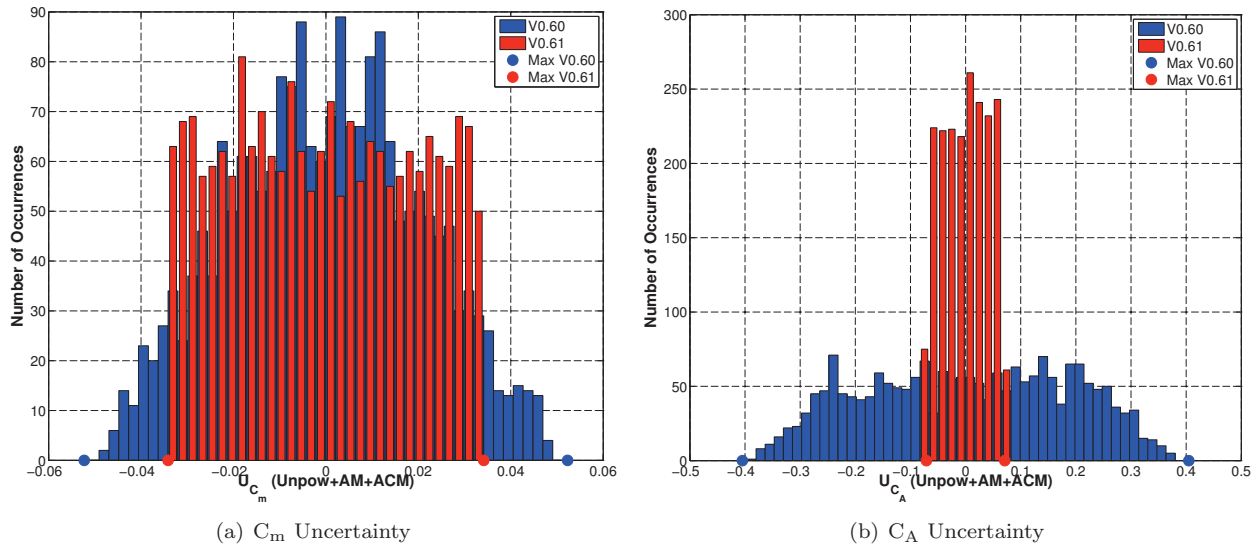
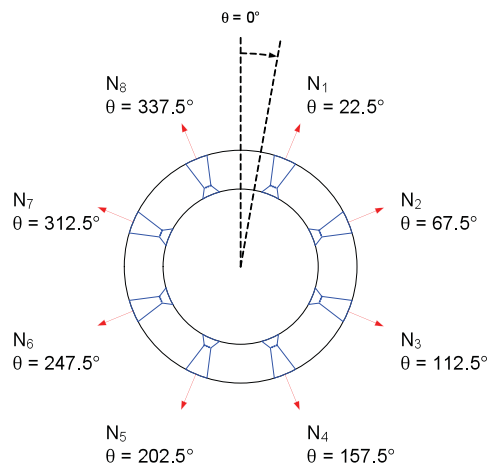


Figure 14. Comparison of histograms for 2,000 random draws of LAV aerodynamic uncertainty between database version 0.60 (increment aero) and version 0.61 (total aero).



(a) Test firing of the ACM



(b) Sketch of ACM nozzle locations, pilot's view

Figure 15. Overview of attitude control motor.

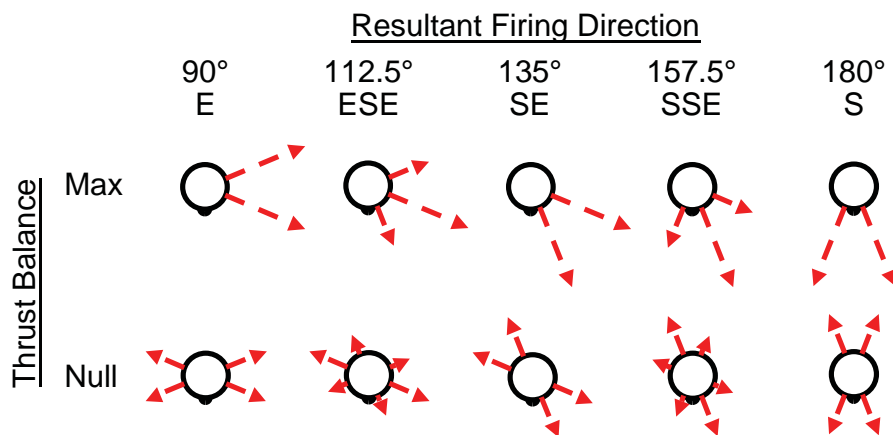


Figure 16. Example ACM thrust allocation profiles.

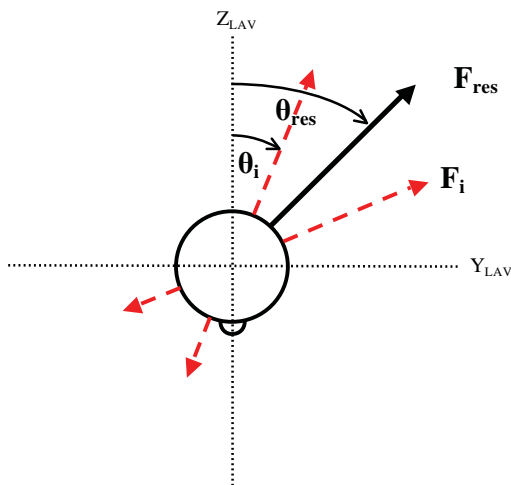
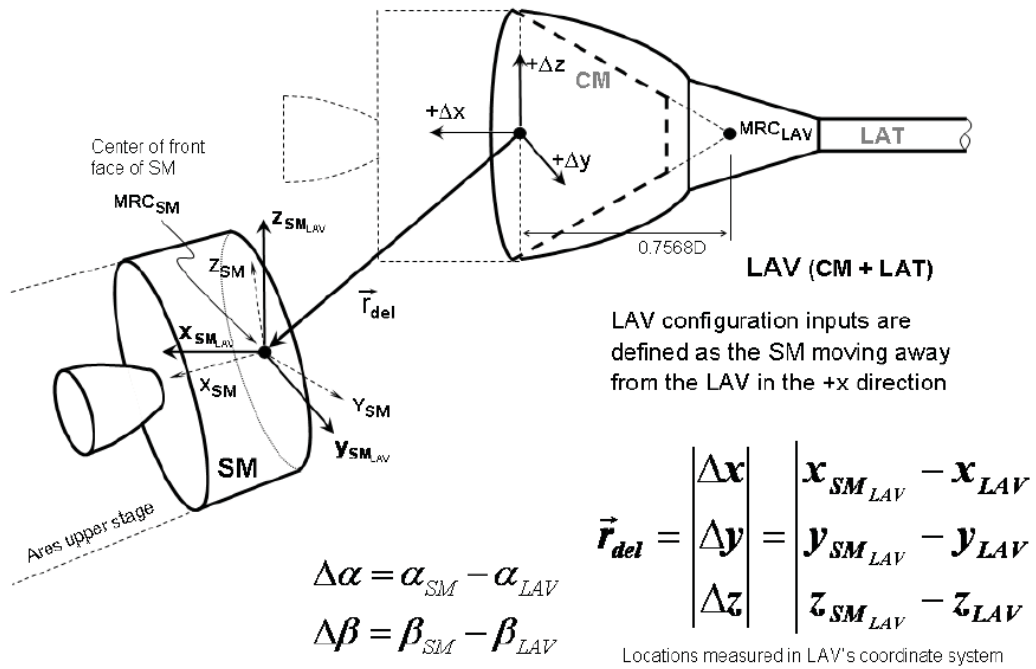
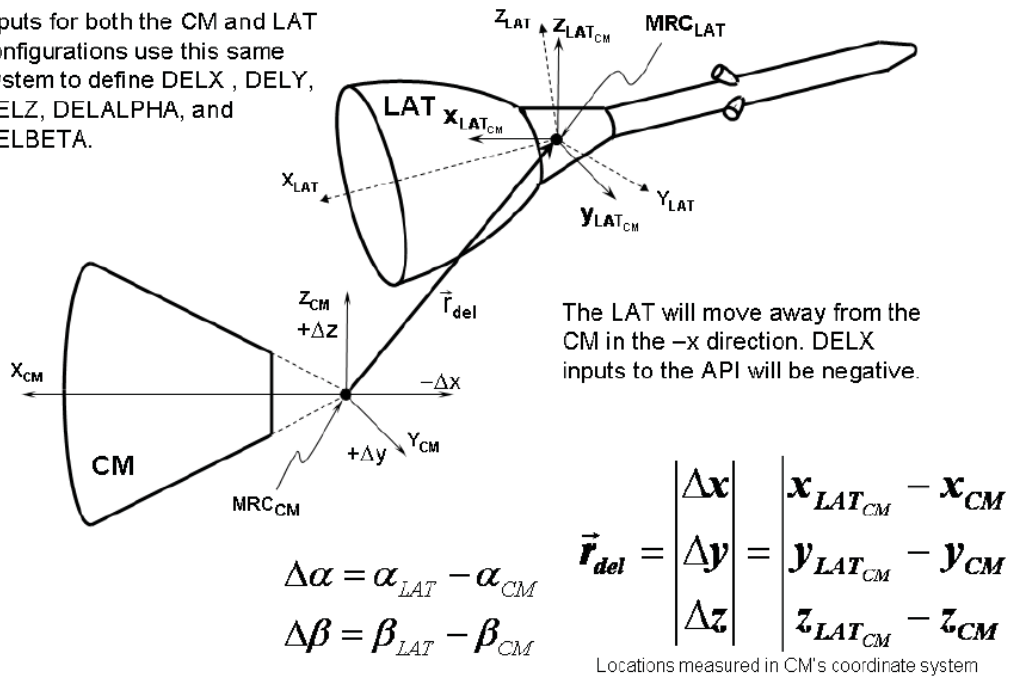


Figure 17. ACM thrust vector definitions.



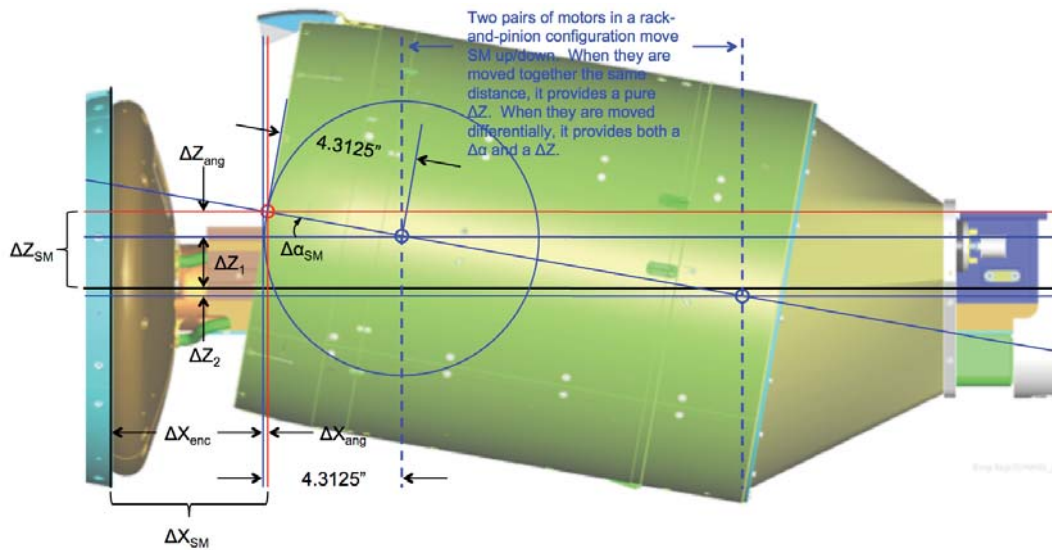
(a) LAV separation from launch vehicle or service module

Inputs for both the CM and LAT configurations use this same system to define DELX, DELY, DELZ, DELALPHA, and DELBETA.

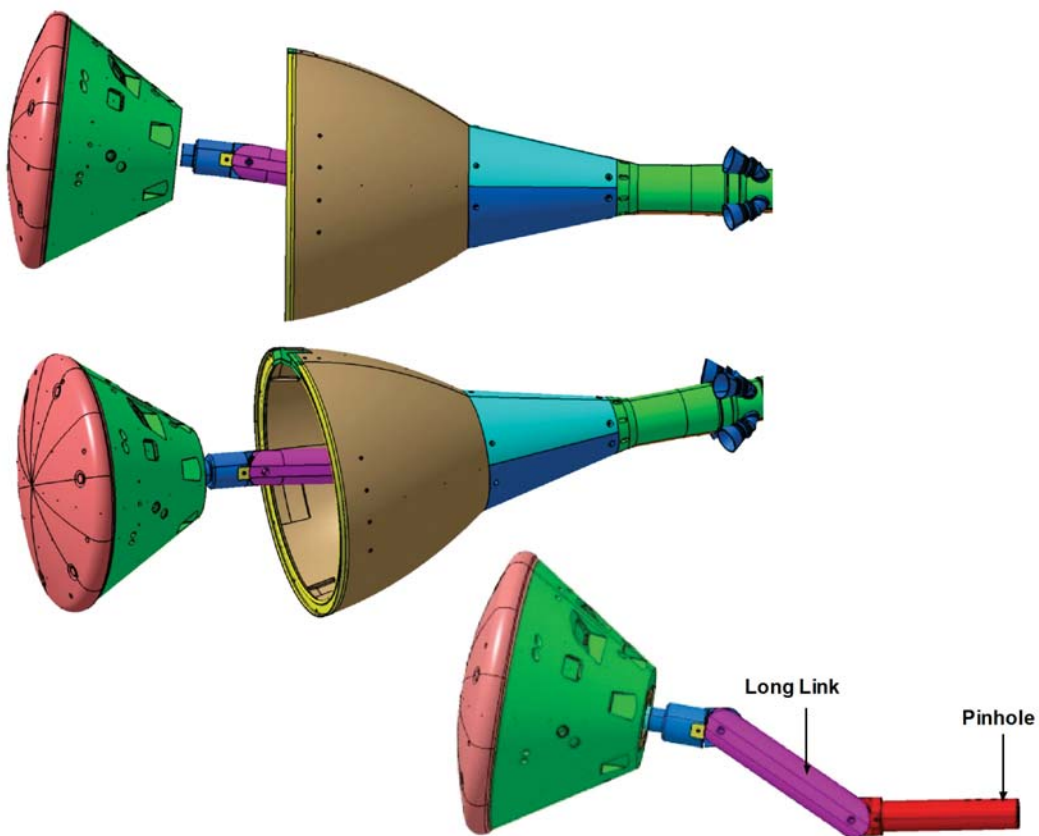


(b) CM separation from LAT

Figure 18. Separation parameter definitions in LAV aerodynamic database.



(a) LAV separation from launch vehicle or service module in wind tunnel test 26-AA



(b) CM separation from LAT in wind tunnel test 24-AA

Figure 19. Examples of vehicle separation mechanisms in CAP wind tunnel tests.

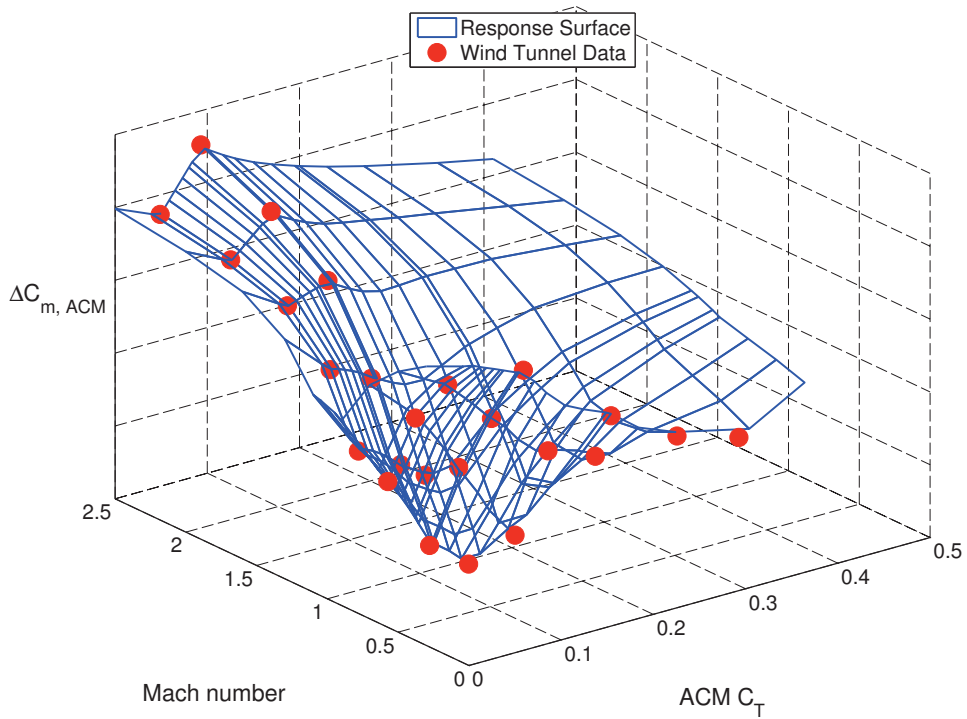


Figure 20. Example response surface fit of wind tunnel data for the ACM pitching moment coefficient increment.

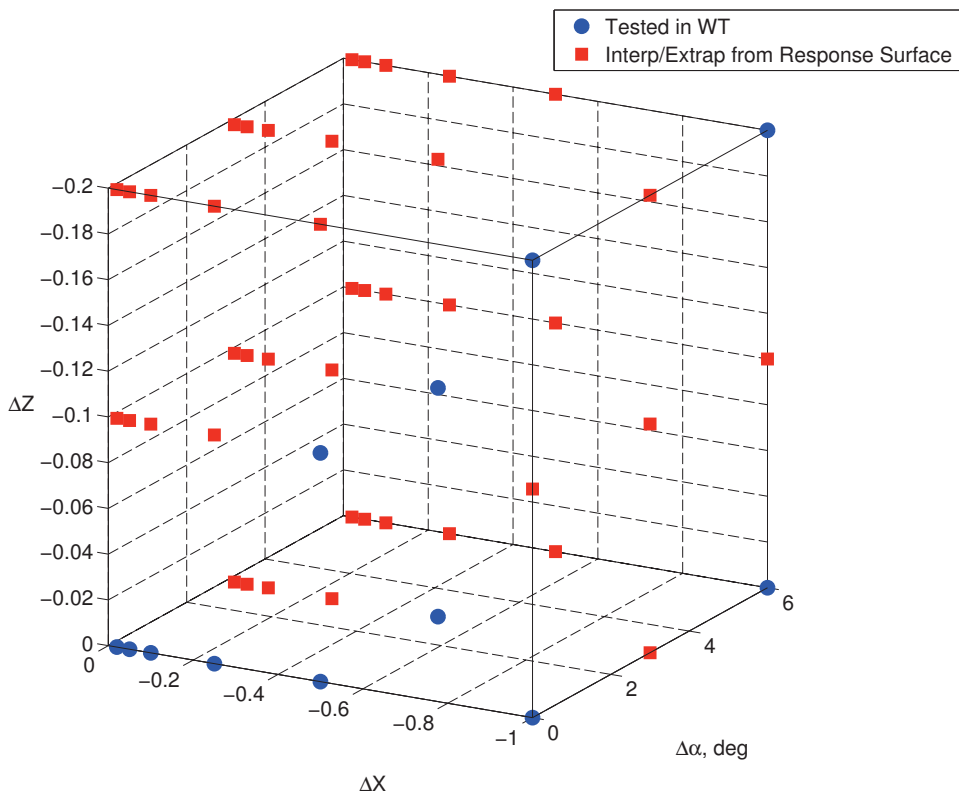


Figure 21. Portions of LAT jettison data space filled in by response surface.

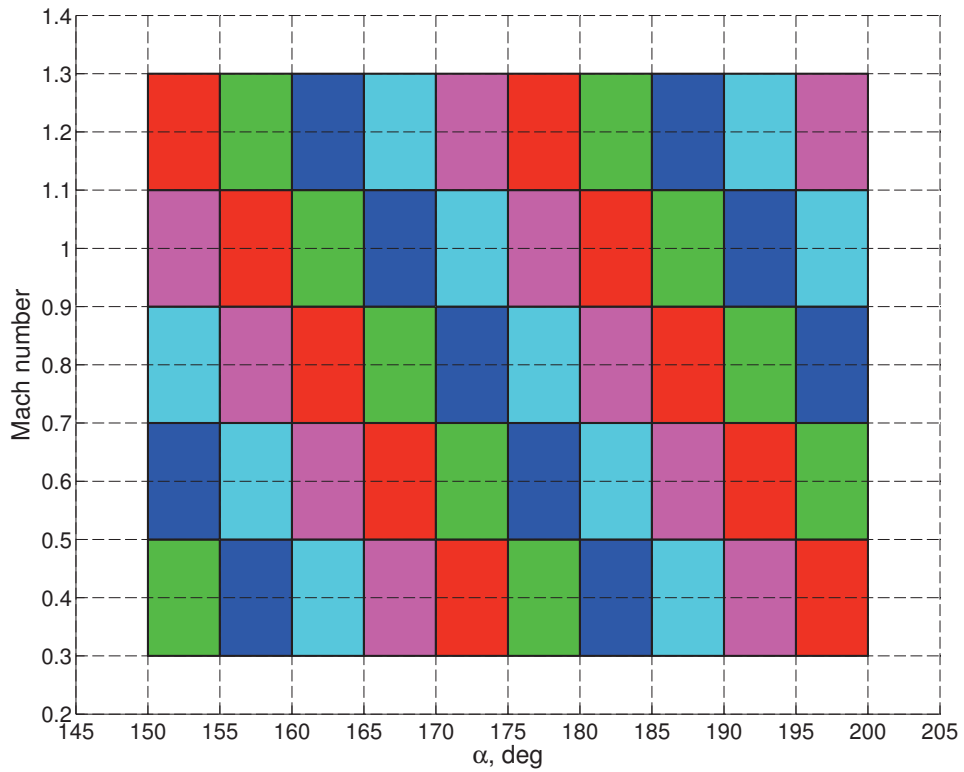


Figure 22. Data space split into overlapping zones of patches.

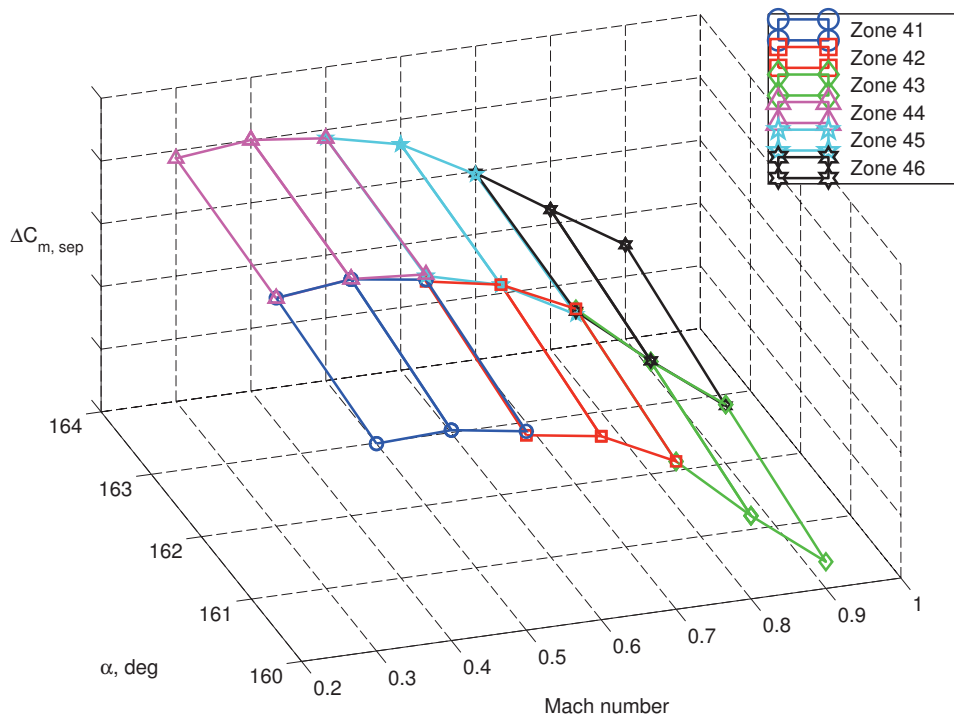


Figure 23. Example showing overlapping response surfaces of wind tunnel data for the CM pitching moment coefficient separation increment.

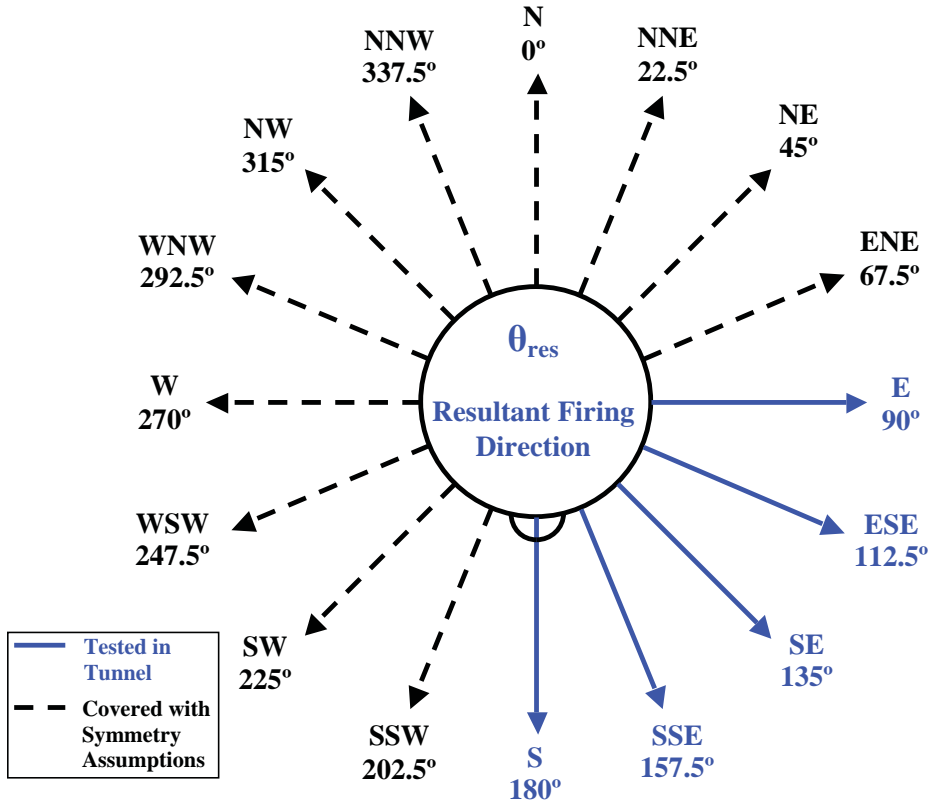


Figure 24. Summary of ACM firing directions tested during coast phase ACM jet interaction wind tunnel tests.

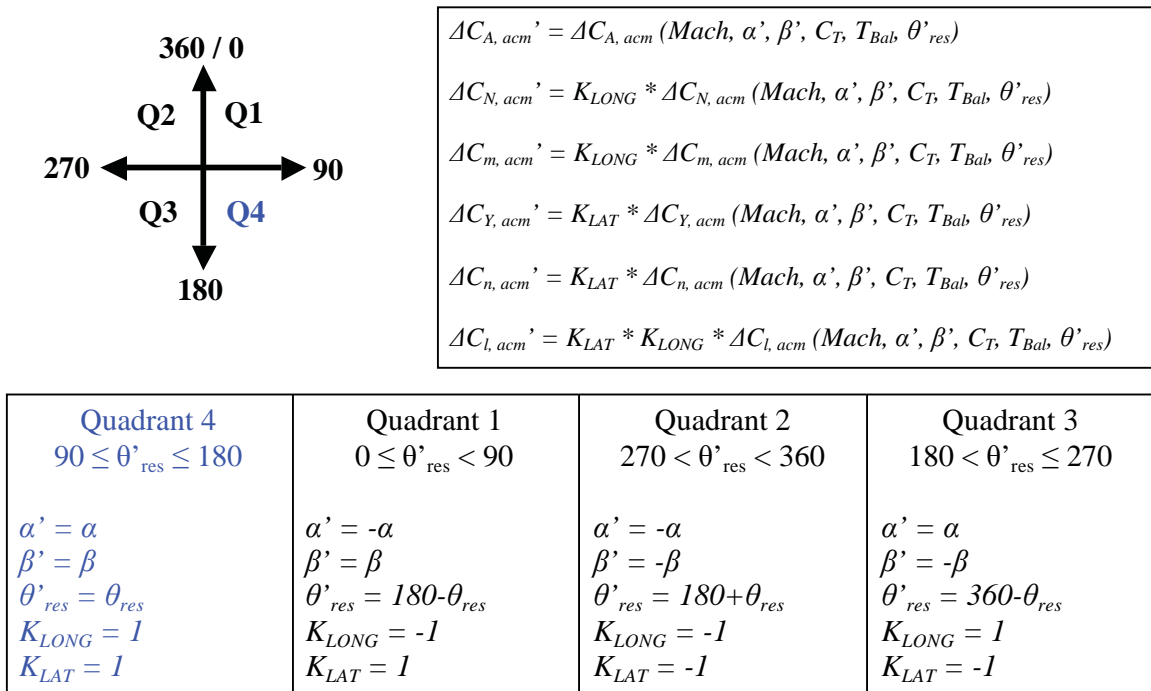


Figure 25. Data reflection rules for mirroring ACM jet interaction increment data for ACM firing directions in quadrant 4 to firing directions in the other quadrants.

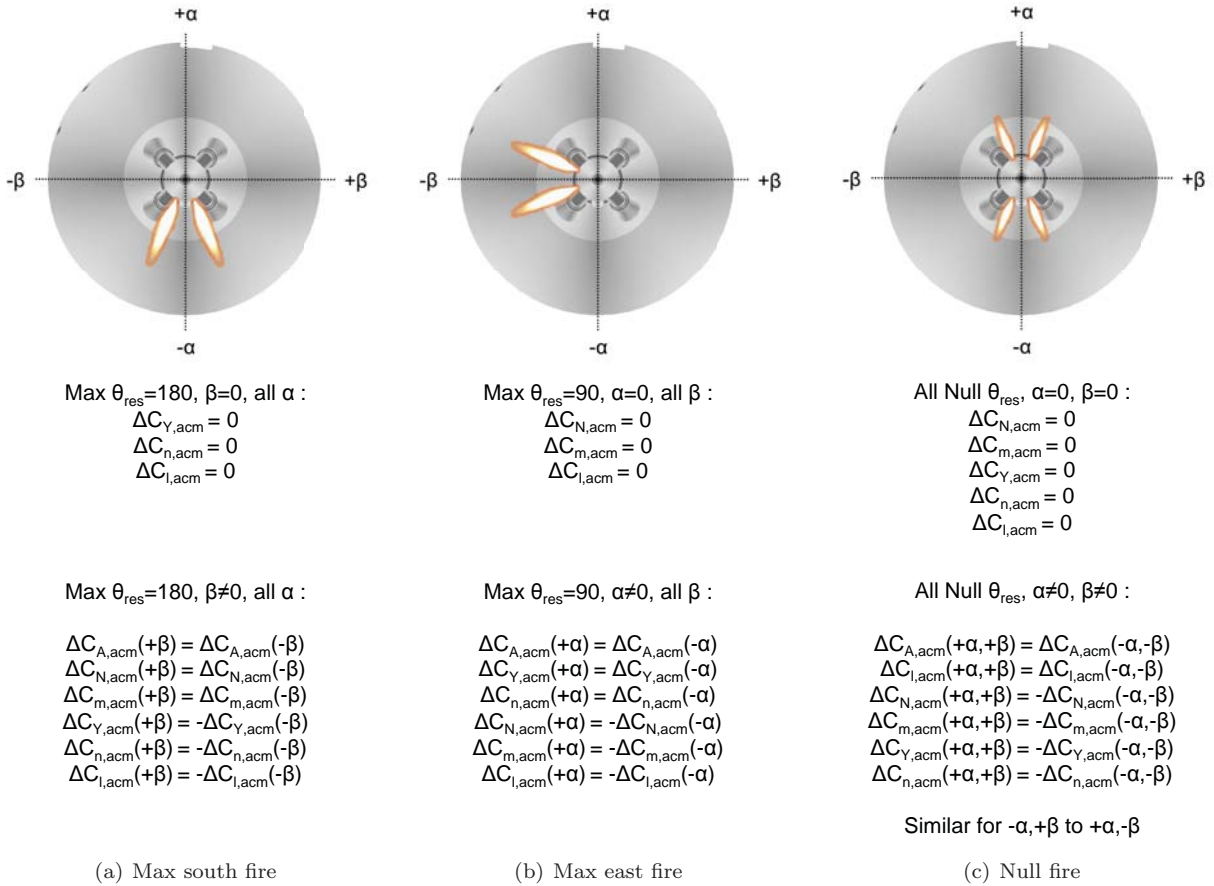


Figure 26. ACM jet interaction data symmetry rules to prevent data inflections when mirroring data.

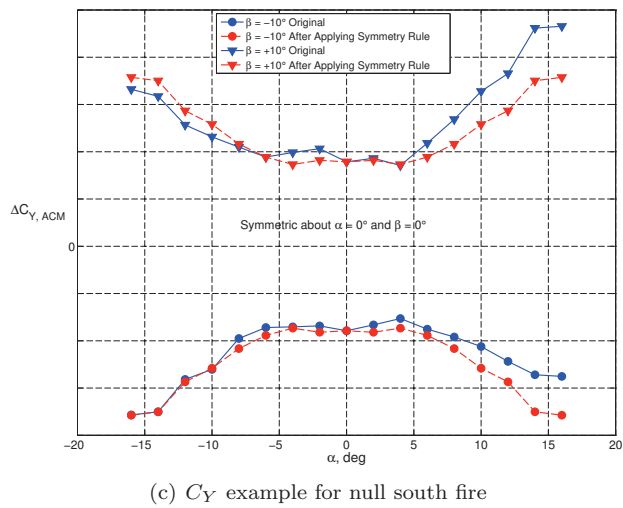
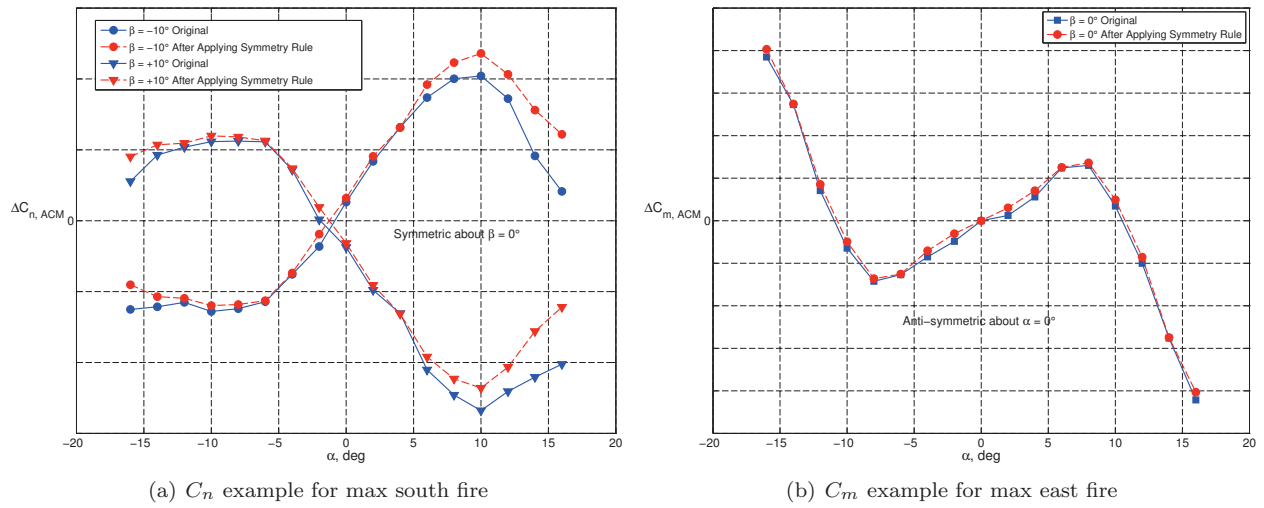


Figure 27. Examples showing application of ACM jet interaction data symmetry rules.

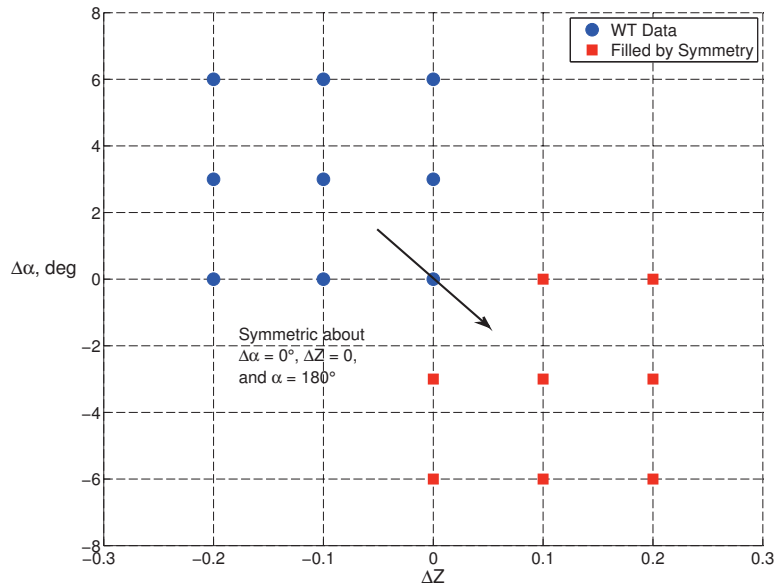


Figure 28. Example of methods used to fill in areas of CM/LAT jettison database not tested in the wind tunnel.

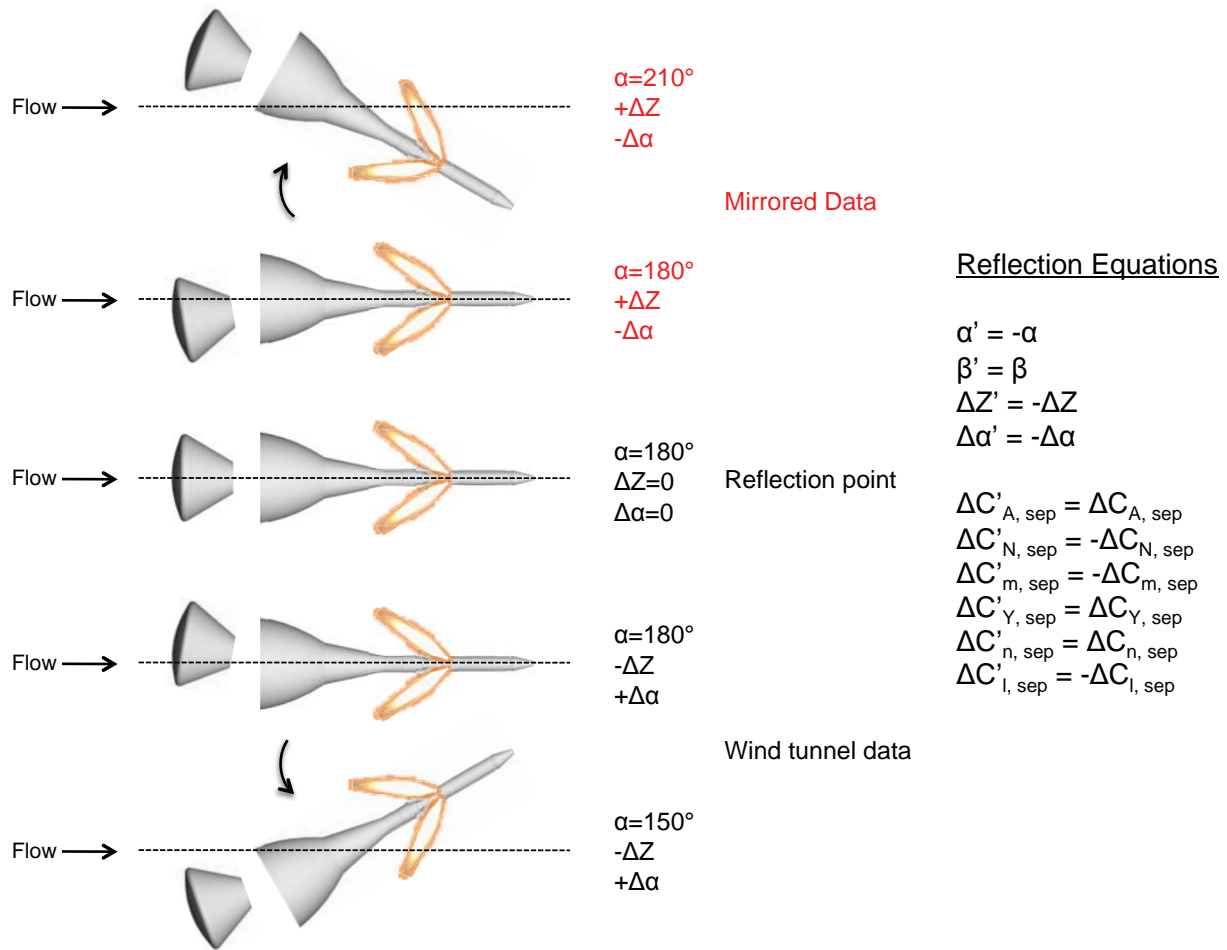


Figure 29. Illustration showing method for mirroring of CM and LAT separation increment data.

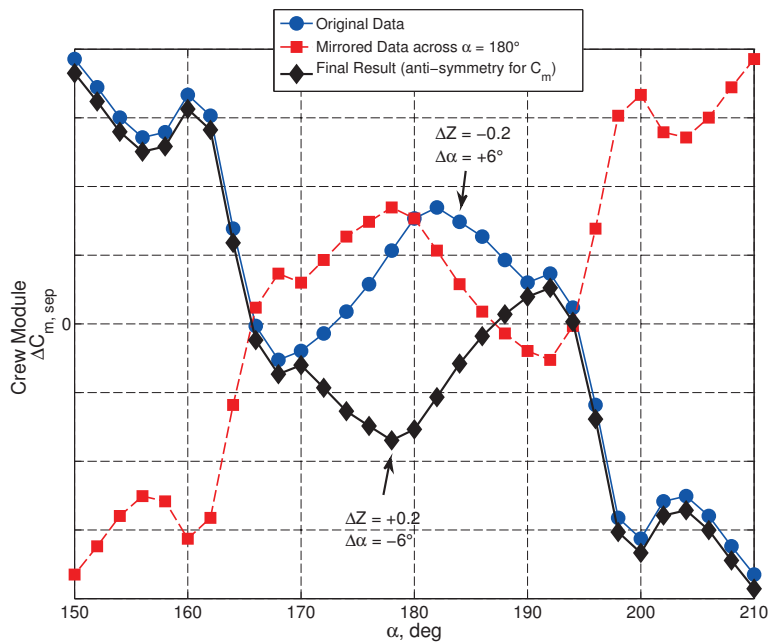


Figure 30. Example showing mirroring of CM separation increment data.